SLAC–PUB–4427
NSF-ITP-87-123
September 1987
T/E/AS

Signal Modulation in Cold Dark Matter Detection*

KATHERINE FREESE[1]†, JOSHUA FRIEMAN[2] AND ANDREW GOULD[2]

[1] *Institute for Theoretical Physics*

University of California, Santa Barbara, California, 93106

[2] *Stanford Linear Accelerator Center*

Stanford University, Stanford, California, 94305

ABSTRACT

If weakly interacting massive particles (WIMPs) are the dark matter in the galactic halo, they may be detected in low background ionization detectors now operating or with low temperature devices under development. In detecting WIMPs of low mass or WIMPs with spin-dependent nuclear interactions (e.g., photinos), a principal technical difficulty appears to be achieving very low thresholds [$\lesssim O(\text{keV})$] in large ($\sim$ kg) detectors with low background noise. We present an analytic treatment of WIMP detection and show that the seasonal modulation of the signal can be used to detect WIMPs even at low signal-to-background levels and thus without the necessity of going to very low energy thresholds. As a result, the prospects for detecting a variety of cold dark matter candidates may be closer at hand than previously thought. We discuss in detail the detector characteristics required for a number of WIMP candidates, and carefully work out expected event rates for several present and proposed detectors.

Submitted to *Physical Review D*

* Work supported by the Department of Energy, contract DE–AC03–76SF00515.

† Present address: Department of Astronomy, University of California, Berkeley, CA 94720

1. Introduction

The observed flatness of spiral galaxy rotation curves strongly suggests that the Milky Way is embedded in a dark halo, which appears to make up 90% of the mass of the galaxy. Several arguments suggest that the dark matter (DM) is not baryonic, but instead may be composed of exotic, stable elementary particles. Elementary particle dark matter candidates may be loosely grouped into two categories, 'hot' and 'cold', corresponding to particles which are relativistic (hot) or non-relativistic (cold) when galaxy scales enter the horizon. The most successful candidate theory of galaxy formation to date assumes that the dark matter is 'cold', so that galaxy scale perturbations are not erased by relativistic free streaming.[1] Furthermore, particle physics models suggest a host of cold dark matter candidates, including massive Dirac or Majorana neutrinos and various particles predicted by supersymmetry, such as scalar neutrinos, photinos, or higgsinos. Generally, the constraint that these particles do not overclose the universe ($\Omega_{DM} \lesssim 2$) requires particle masses $m_{DM} \gtrsim O(\text{GeV})$ (an exception is the invisible axion). Clearly, a crucial test of the cold dark matter theory is to find direct evidence for or against the existence of such weakly interacting massive particles (WIMPs).

At present, there are significant astrophysical and experimental constraints on cold dark matter candidates. WIMPs in the halo would be captured by the sun (if $m_W \gtrsim 3$ GeV) and the earth (for $m_W \gtrsim 12$ GeV), where they would annihilate, and could give rise to an observable high energy neutrino signal in proton decay detectors.[2] If WIMPs constitute the halo, the absence of such a signal implies that either:

i) the WIMP scattering and annihilation rates in the sun and earth are both sufficiently low that the neutrino signal is below the present sensitivity of proton decay detectors,

ii) the WIMP annihilation cross-section must be suppressed compared to its nuclear scattering rate (e.g., Majorana fermions with p-wave suppressed

annihilation), or

iii) the universe carries a net asymmetry of WIMPs, so that only a small number of anti-particles are captured (e.g., Dirac fermions or complex scalars).

In addition, WIMPs more massive than $O(20\text{ GeV})$ which have coherent (spin-independent) interactions with nuclei (e.g., Dirac neutrinos, scalar neutrinos) would have been seen in ultralow background double beta decay detectors (again assuming a halo density of WIMPS).[3] These experiments leave open the possibility that the halo may comprise either less massive particles, $m_W \lesssim 20$ GeV, or particles which have only spin-dependent interactions with nuclei, e.g., photinos and Majorana neutrinos.

Recently, there have been several proposals to build low temperature devices for the direct detection of cold dark matter candidates in the galactic halo.[4,5] A new generation of such cryogenic detectors will be required in order to reach sensitivity to target nuclei recoiling with energies $\lesssim O(\text{keV})$ due to elastic scattering of $O(\text{GeV})$-mass halo particles. Proposed experimental ideas include superheated superconducting colloids and crystal bolometers. Depending on the design, these detectors may simply register all particles depositing energy above some threshold, or they may directly measure the energy of the incoming particles. In this paper, we consider detectors operating in both threshold and energy-sensitive modes.

Our general analysis in this paper is applicable to both conventional ionization and cryogenic detectors.

Given the ubiquity of background sources, these detectors can be used to set upper limits on the halo WIMP density more easily than to positively detect WIMPs. Suppose, for example, that a detector is designed so that the expected background count rate is of order 2 per day. And suppose that, from theory, one knows that a halo mass density of 3 GeV photinos will produce a signal of 4 per day. Now in an experiment it is found that there are 2 events per day. One may use this to put an upper bound on the density of 3 GeV photinos of 50%

of halo density. Suppose instead, however, that the experiment yields 5 events per day. One possible interpretation is that the background is 2 per day and the density of 3 GeV photinos is about 75% of halo density. But another possible, and *a priori* more likely, interpretation is that the experimenter underestimated the background. Thus, finding positive evidence for a halo density of WIMPs appears to rest critically on a belief in the experimenter's claims about background.

To remedy this situation, one would like a clear signature which distinguishes the WIMP signal from other sources of background. Drukier, Freese, and Spergel[5] showed that, due to the earth's motion around the sun, the WIMP signal would have an annual sinusoidal modulation which peaks in late spring. Thus, they showed it would be possible, in principle, to demonstrate that the data was not pure background.[6]

In this paper, we analyze in detail the conditions under which one can measure the modulation of the WIMP signal. We also emphasize a different attitude toward the usefulness of modulation. In ref.5, modulation was viewed as a method of confirming a suspected WIMP signal; given this point of view, WIMP detection requires a large signal to noise ratio, and thus a reliable understanding of background levels. We argue that modulation can itself be used as the *primary* means of detecting WIMPs (rather than as a confirmation), even in the presence of large backgrounds (i.e., backgrounds comparable to or even larger than the WIMP signal). As a result, the prospects for detection of particles such as Majorana fermions, which generally have only spin-dependent interactions with nuclei and thus relatively small cross-sections, appear more promising than previously thought. Thus, a clear understanding of modulation is important not only in the analysis of data, but also in the design of experiments.

Heretofore, modulation has not been seen as a primary means of detecting WIMPs for two reasons. First, modulation is a small effect compared to the absolute count rate, and thus one naively expects its detection to require many events and long counting times. However, even a small *periodic* component of

data superposed with a much larger random component can be extracted by a correlation analysis. Second, previous authors tended toward the belief (erroneous, as we will show) that modulation can be measured only at very high detector recoil energies, for which the signal count rate is severely reduced. This belief is based on the fact that the modulation, relative to the average WIMP signal, increases as the threshold energy of the detector is raised. We show below, however, that a more significant statistical measure of the modulation is maximized at comparatively low thresholds.

In Sec.II, we present an analytic treatment of WIMP detection and modulation, using an approximate halo model. In Sec.III, we discuss the statistics of modulation and the prerequisites for its statistically significant detection. The reader interested only in our numerical results may skip to Sec.IV, where we present useful, general expressions for signal and modulation rates, under different assumptions about background levels. In Sec.V, we apply the analysis to find event rates for a variety of WIMP candidates for several present and proposed detectors, and present our results graphically. Sec.VI contains our brief conclusions, and some of the technical details are relegated to the Appendices.

2. Analytic Theory Of WIMP Detection

The rate of WIMP detection can be obtained by folding in the flux of WIMPs with the probability of their interacting in the detector. For particles with speed w with respect to the earth and a detector with threshold energy ϵ, the rate of WIMP detection per unit volume V of detector is

$$\frac{I(\eta,\epsilon)}{V} = \int dw\ f_\eta(w)\Omega_\epsilon(w)\ . \tag{2.1}$$

Here $f_\eta(w)$ is the speed distribution of WIMPs in the earth's frame [the number density of WIMPs with speed in the range $(w, w+dw)$], and $\Omega_\epsilon(w)$ is the rate per unit time that a WIMP with speed w scatters with energy loss at least ϵ,

when it is travelling through the detector medium. The parameter η is defined below.

The form of the halo distribution function presumably depends upon the details of the collapse process which formed the galaxy. However, general dynamical arguments suggest that the WIMP velocities were 'thermalized' by fluctuations in the gravitational potential during collapse, a process known as violent relaxation.[7] On this basis, we will assume the WIMPs have an approximately Maxwell-Boltzmann speed distribution in the galactic rest frame (the halo is assumed to be non-rotating),

$$f_0(v)dv = 4\pi n_W \left(\frac{3}{2\pi\bar{v}^2}\right)^{3/2} v^2 \exp\left(-\frac{3v^2}{2\bar{v}^2}\right) dv \ , \tag{2.2}$$

where $\bar{v}$ is the halo velocity dispersion, discussed below, n_W is the local number density of WIMPs of mass m_W, and the halo density is $\rho_{halo} = n_W m_W = 0.007 M_\odot/pc^3 = 0.4\text{GeV/cm}^{-3}$ [8] (there is a factor 2 uncertainty in this estimate). Equation (2.2) corresponds to an infinite isothermal sphere, and is consistent with a self-gravitating halo with a density profile $\rho \sim r^{-2}$, which yields a flat rotation curve at large radii.

In actuality, the WIMP distribution will be truncated at the (local) galactic escape velocity, $v_{esc} \simeq 500 - 650$ km/sec, and in addition may be anisotropic. For example, an anisotropy in the halo distribution is likely to arise from the partial infall of the dark matter into the gravitational potential of the baryons in the galactic bulge and disk.[9] However, Drukier, Freese and Spergel[5] showed that the modulation is not qualitatively affected by a small anisotropy, and we show in Appendix I that truncation at the escape velocity likewise has little impact *if detector thresholds are sufficiently low.* These modifications to the distribution function will yield only small quantitative corrections to the results presented in this paper. Until detailed models of the halo are more fully developed, we will take Equation (2.2) as a provisional choice, which has the advantage that detection rates can be given in completely analytic form. The results given here can

obviously be extended, at least numerically, to more complicated distributions, which we plan to do in a subsequent publication. (If WIMPs *are* detected, it would clearly be important to design experiments to probe the detailed structure of the halo distribution.)

To convert Equation (2.2) into the distribution seen by an observer moving with the velocity of the earth, $v_\oplus$, we make the galilean transformation, $\vec{v} = \vec{w} + \vec{v}_\oplus$, where w is the WIMP speed with respect to the earth. In the earth's frame, the WIMPs then have a speed distribution[10]

$$f_\eta(w)dw = \frac{4}{\pi^{\frac{1}{2}}} n_W x^2 \exp[-(x^2+\eta^2)] \frac{\sinh(2x\eta)}{2x\eta} dx \ , \tag{2.3}$$

where x is the dimensionless WIMP speed (with respect to the earth) and η is the dimensionless earth speed with respect to the halo,

$$x^2 = \frac{3w^2}{2\bar{v}^2} \ , \qquad \eta^2 = \frac{3v_\oplus^2}{2\bar{v}^2} \ . \tag{2.4}$$

For an isothermal system, the circular velocity (e.g., of stars in the galactic disk) is related to the three-dimensional velocity dispersion by

$$v_{circ}^2/\bar{v}^2 = 2/3 \ . \tag{2.5}$$

Since the average local circular velocity about the galactic center (the rotational speed of the local standard of rest(LSR)) is[11] $v_{circ} = 220 \pm 20$ km/sec, we estimate the halo velocity dispersion $\bar{v} = 270 \pm 25$ km/sec. Correcting for the motion of the sun with respect to the LSR,[11] we also find the net speed of the sun with respect to the galactic rest frame is $v_\odot = 232 \pm 20$ km/sec. Using Equations (2.4) and (2.5), it follows that the yearly average value of η is $\eta_0 = 1.05$. The orbital speed of the earth around the sun is 30 km/sec, and the angle between the axis of its orbit and the velocity vector of the sun is approximately[12] $\delta =$

30.7° ($\sin\delta = 0.51$). Thus η may be expressed as a function of time,

$$\eta(t) = \eta_0 + \Delta\eta\cos(\omega t) \tag{2.6}$$

where

$$\Delta\eta = .07 \pm .01\ , \qquad \omega = \frac{2\pi}{\mathrm{yr}}\ , \tag{2.7}$$

and t is taken to be zero when the earth's speed is at a maximum, in May.

The energy lost by a WIMP with speed w in elastic scattering with a nucleus of mass M is

$$\Delta E = \frac{m_W^2 M}{(m_W + M)^2} w^2 (1 - \cos\theta)\ , \tag{2.8}$$

so that

$$\left(\frac{\Delta E}{E}\right)_{max} \equiv g(m_W, M) = \frac{4 m_W M}{(m_W + M)^2}\ . \tag{2.9}$$

Thus, $g(m_W, M) \leq 1$, and the upper limit is achieved when the WIMP and nuclear masses are matched. For low energy, isotropic scattering, it follows from Equation (2.8) that the probability distribution for energy loss in a collision, $P(\Delta E/E)$, is flat over the interval $0 \leq (\Delta E/E) \leq g(m_W, M)$, or $P(\Delta E/E) = g^{-1}$. The scattering function Ω is obtained by integrating over this probability distribution from the threshold, $(\Delta E/E) \geq (\epsilon/E)$, and is given by[5,10]

$$\Omega_\epsilon(w) = \sigma n_N w \int_{2\epsilon/m_W w^2}^{g(m_W, M)} g(m_W, M)^{-1} \exp(-\Delta E/E_0)\, d\left(\frac{\Delta E}{m_W w^2/2}\right)\ , \tag{2.10}$$

where n_N is the number density of target nuclei and σ is the low-energy interaction cross-section. The exponential factor in the integrand takes into account the loss of coherence in WIMP-nucleus interactions for momentum transfers comparable to or larger than the inverse nuclear radius.[13] Here, E_0 is the nuclear

'coherence energy',

$$E_0 \equiv \frac{3\hbar^2}{2MR^2} , \tag{2.11}$$

where R^2 is the mean square radius of the nucleus,[14]

$$R \simeq \left[.91 \left(\frac{M}{GeV} \right)^{1/3} + .3 \right] \times 10^{-13} \text{cm} . \tag{2.12}$$

Equation (2.10) may be easily evaluated

$$w\Omega_\epsilon(w) = \frac{2\sigma n_N E_0}{m_W g} \left[\exp\left(-\frac{\epsilon}{E_0} \right) - \exp\left(-\frac{\Delta E_{max}}{E_0} \right) \right] . \tag{2.13}$$

It is convenient to define the new variables

$$b \equiv \frac{g m_W \bar{v}^2}{3E_0} , \qquad A^2 \equiv \frac{3\epsilon}{g m_W \bar{v}^2} , \tag{2.14}$$

in terms of which Equation (2.13) becomes

$$w\Omega_\epsilon(w) = \frac{\sigma n_N}{b} \frac{2}{3} \bar{v}^2 [\exp(-bA^2) - \exp(-bx^2)] . \tag{2.15}$$

The parameter b is the maximum energy loss of a 'typical' halo WIMP as a fraction of the coherence energy; for $b \ll 1$, the departure from coherence is negligible. This parameter may be estimated to be

$$b = \frac{0.83 \left(\frac{m_W}{40\ GeV} \right)^2}{\left(\frac{m_W}{M} + 1 \right)^2} \left[\left(\frac{M}{200 GeV} \right)^{\frac{1}{3}} + .06 \right]^2 \bar{v}_{270}^2 , \tag{2.16}$$

which we show for the reader's convenience in Fig.1. The parameter A^2 is roughly the ratio of the threshold energy to the maximum energy loss of a typical WIMP, and is given by

$$A^2 = \frac{4.6 \times 10^{-2}}{\bar{v}_{270}^2} \left(1 + \frac{M}{m_W} \right)^2 \left(\frac{\epsilon}{keV} \right) \left(\frac{M}{20\ GeV} \right)^{-1} . \tag{2.17}$$

This is shown in Fig.2 for a variety of WIMP and nuclear masses. Note that, for targets with large atomic number, A^2 is a sensitive function of the WIMP mass.

From Fig.1, we see that in most cases of interest, $b \ll 1$, and equation (2.15) takes the simple form

$$w\Omega_\epsilon(w) = \sigma n_N \frac{2}{3}\bar{v}^2(x^2 - A^2). \tag{2.18}$$

We will assume that this limit holds in the remainder of the body of this paper. However, it must be noted that when b is not small, i.e., for heavy detector nuclei and relatively large WIMP masses, the conclusions of the paper must be radically revised. The analysis for arbitrary b is discussed in Appendix II, where we show that the modulation is suppressed for large b.

Using Equations (2.3) and (2.18), we may now evaluate the detection rate, equation (2.1),

$$I(\eta(t),\epsilon) = \left(\frac{8}{3\pi}\right)^{\frac{1}{2}} \frac{\sigma N_N n_W \bar{v}}{2\eta}\left[(-A_-A_+ + \frac{1}{2})\chi(A_-,A_+) + \frac{1}{2}[A_+ e^{-A_-^2} - A_- e^{-A_+^2}]\right] \tag{2.19}$$

where

$$A_\pm = A \pm \eta \ , \tag{2.20}$$

$$\chi(x_1,x_2) \equiv \int_{x_1}^{x_2} dy e^{-y^2} = \frac{\sqrt{\pi}}{2}[\mathrm{erf}(\mathrm{x}_2) - \mathrm{erf}(\mathrm{x}_1)] \ , \tag{2.21}$$

and N_N is the number of nuclei in the detector. Since $\Delta\eta \ll \eta_0$, the detection rate is accurately given by the lowest order terms in the Taylor series

$$I(\eta(t)) = I(\eta_0) + \left(\frac{\partial I}{\partial \eta}\right)_{\eta_0} \Delta\eta \cos(\omega t) + \ldots \ , \tag{2.22}$$

where the first term represents the time-averaged WIMP signal. In evaluating this term, we note that $I(\eta_0 = 1.05)$ differs significantly from $I(\eta = 0)$, e.g., by

$O(30\%)$ at zero threshold ($A^2 = 0$), so that it is *not* a good approximation to estimate the time-averaged WIMP signal by considering the detector as stationary with respect to a Maxwell-Boltzmann distribution. The second term in Equation (2.22) we call the absolute modulation, and it is given explicitly by

$$\frac{S_m \cos(\omega t)}{\text{year}} \equiv$$
$$\Delta\eta I(\eta_0, \epsilon)\cos(\omega t)\left[\frac{2\eta_0\chi(A_-, A_+) + e^{-A_+^2} + e^{-A_-^2}}{(-A_-A_+ + \frac{1}{2})\chi(A_-, A_+) + \frac{1}{2}(A_+e^{-A_-^2} - A_-e^{-A_+^2})} - \frac{1}{\eta_0}\right]. \tag{2.23}$$

The time-averaged WIMP signal and the absolute modulation as functions of the threshold (normalized to their values at $A = 0$) are shown as the functions $\gamma(A^2)$ and $\beta(A^2)$ in Fig.5. (The function γ is given by the bracketed expression in Equation (2.19), divided by its value at $A = 0$; the function β is the product of the bracketed expressions in Equations (2.19) and (2.23), also divided by its value at $A = 0$. Numerical expressions for the average count rate and modulation are given in section IV.) As expected, of course, the average signal drops monotonically with increasing threshold. More surprising, perhaps, is the fact that the absolute modulation peaks near $A \simeq 1$, i.e., where the threshold energy is tuned to the maximum energy loss of typical WIMPs. On the other hand, the relative modulation, the ratio of the absolute modulation to the average signal ($\sim \beta/\gamma$), grows monotonically with increasing threshold, as found in Ref.5. However, as we discuss in the next section, neither the absolute nor the relative modulation is the most relevant quantity to be considered.

3. Statistics Of Modulation

We consider a year long experiment in which the *daily* signal and background are represented by random variables $S(t)$ and $B(t)$ respectively. The background will be assumed to be a Poisson random variable, which implies that its variance is equal to its mean,

$$\sigma^2(B) = \langle B \rangle \ . \tag{3.1}$$

As discussed in the previous Section, the WIMP signal will be assumed to be composed of two parts,

$$S(t) = S_0(t) + \left(\frac{S_m}{365}\right) \cos(\omega t) \ . \tag{3.2}$$

The first term, S_0, is a Poisson random variable,

$$\sigma^2(S_0) = \langle S_0 \rangle \ , \tag{3.3}$$

and the second term in Equation (3.2) is the absolute annual modulation, expressed as a daily rate. Strictly speaking, $S_m/365$ should be treated as a random variable, but since, in cases of interest, $(S_m/365) \ll \langle S_0 \rangle$, the modulation S_m may be treated as a constant, i.e., its variance may be neglected. The daily rate of data is then

$$D(t) \equiv S(t) + B(t) = S_0(t) + B(t) + \left(\frac{S_m}{365}\right) \cos(\omega t) \ . \tag{3.4}$$

For convenience, we also define the random variables representing the *annual* signal, background, and data,

$$S_{tot} \equiv \sum_{\text{all year}} S(t) \ , \quad B_{tot} \equiv \sum_{\text{all year}} B(t), \quad D_{tot} \equiv \sum_{\text{all year}} D(t) \ . \tag{3.5}$$

We note that

$$\sigma^2(S_{tot}) = \langle S_{tot}\rangle = 365\langle S_0\rangle \ , \quad \sigma^2(B_{tot}) = \langle B_{tot}\rangle = 365\langle B\rangle \ , \tag{3.6}$$

and

$$\sigma^2(D_{tot}) = \langle D_{tot}\rangle = \langle S_{tot}\rangle + \langle B_{tot}\rangle \ . \tag{3.7}$$

We wish to extract information about the modulation, S_m, from measurements of the data, $D(t)$. To accomplish this, we define the random variable

$$X \equiv \sum_{\text{all year}} 2\cos(\omega t)D(t) \ , \tag{3.8}$$

which projects out the modulating portion of the data. Simple statistics tells us

$$\langle X\rangle = S_m, \quad \sigma^2(X) = 2\langle D_{tot}\rangle = 2(\langle S_{tot}\rangle + \langle B_{tot}\rangle) \ . \tag{3.9}$$

This evaluation leads us to define a new random variable R, the *modulation significance*,

$$R \equiv \frac{X}{\sqrt{2\langle D_{tot}\rangle}} \ . \tag{3.10}$$

If $\langle D_{tot}\rangle \gg 1$, then, to an excellent approximation,

$$r \equiv \frac{x}{\sqrt{2d_{tot}}} \tag{3.11}$$

may be regarded as a measurement of R; here x and d_{tot} are respectively measurements of X and D_{tot}. *For pure noise* ($S_m = 0$), R is a (nearly) Gaussian random variable with zero mean and unit variance,

$$p_n(r)dr = \frac{1}{\sqrt{2\pi}}e^{-r^2/2}dr \ . \tag{3.12}$$

The modulation significance R is precisely what we want to measure, because it contains both phase and amplitude information about the signal and

has simple statistical properties. If a measurement of R yields the value r_0, it will be generated by a real modulation in the signal (as opposed to noise) with confidence level

$$\text{C.L.} = 1 - \int_{r_0}^{\infty} p_n(r)dr = \frac{1}{2} + \frac{1}{2}\text{erf}\left(\frac{r_0}{\sqrt{2}}\right) . \tag{3.13}$$

For reference, we list several values of r_0 with their respective confidence levels: $r_0 = 1(84\%)$, $1.29(90\%)$, $1.64(95\%)$, $2(97\frac{1}{2}\%)$, and $3(99\frac{1}{2}\%)$. That is, a measurement of $r_0 = 1.3$ would be a fairly reliable indicator of modulation and a measurement of $r_0 = 2$ would be a very reliable indicator.

It is instructive to compare the foregoing analysis with the standard power spectrum, or periodogram, analysis.[15] In a power spectrum analysis, the relevant discrete data variable is

$$\tilde{D}(t_j) = S_0(t_j) - \langle S_0 \rangle + B(t_j) - \langle B \rangle + \left(\frac{S_m}{365}\right)\cos(\omega_0 t_j) , \tag{3.14}$$

which we consider as the sum of a Gaussian 'noise' term (with zero mean) and a periodic signal. If the data are binned into days and the experiment counts for N_0 days, the periodogram is defined as the absolute square of the discrete Fourier transform,

$$P_{\tilde{D}}(\omega) = \frac{1}{N_0}\left|\sum_{j=1}^{N_0} \tilde{D}(t_j)\exp(-i\omega t_j)\right|^2 . \tag{3.15}$$

At the signal frequency ω_0, the expected value of the power due to the signal is

$$P_{S_m} = \frac{N_0}{4}\left(\frac{S_m}{365}\right)^2 , \tag{3.16}$$

and the power due to the noise is just the total variance,

$$P_n = \sigma^2(S_0) + \sigma^2(B) = \frac{\langle D_{tot} \rangle}{365} . \tag{3.17}$$

Thus, for one year of data, the signal-to-noise ratio is

$$\langle Q \rangle = \frac{P_{S_m}}{P_n} = \frac{\langle R \rangle^2}{2} . \tag{3.18}$$

For Gaussian noise, the power at a given frequency has an exponential probability distribution,

$$p_n(Q)dQ = \exp(-Q)dQ \ , \tag{3.19}$$

(note that Q is measured in units of the variance of the noise), so the statistical significance of an observed power z at a selected frequency is just $Pr(Q > z) = \exp(-z)$.

Suppose that a measurement of the modulation significance yields $R = 1$, or $Q = 0.5$. According to Equation (3.13), the confidence that this measurement is due to signal is 84%, while the power spectrum analysis yields a statistical significance, according to Equation (3.19), of only 61%, a far lower confidence level than the method given above. The reason for the reduced confidence of the power analysis is two-fold. First, the power Q does not discriminate between positive or negative values of the amplitude R; clearly, however, a negative measurement of R should be rejected as noise. Second, the fourier transform (3.15) degrades information about the phase of the signal, which is retained in the cosine transform (3.8). Thus, in looking for a signal of *known* frequency and phase, the variable R is more useful than the conventional signal-to-noise ratio.

The reader, aware that 2-σ and even 3-σ bumps on a power spectrum are notoriously unreliable, may be tempted to regard the foregoing confidence level claims as absurdly optimistic. It should be recalled however, that in the analysis of power spectra, one typically asks how much power there is at N different frequencies. That is, one actually conducts N independent experiments. Consequently, there is a strong likelihood (or high false alarm probability) that one or several of these experiments will yield a 2-σ or 3-σ result, even in the absence of an underlying signal. Such results are rightly received with skepticism. By contrast, the analysis given above attempts to answer only one question, not N.

It is also important to emphasize that the significance of these measurements does not depend in any way on the relative magnitude of the signal and background. The only assumption which has been made about the background is that it is unmodulated (or, more precisely, has no near-annual component to its modulation). This assumption is surely reasonable and, in any event, can be partially checked by measuring the annual component of modulation orthogonal to X:

$$Y \equiv \sum_{\text{all year}} 2\sin(\omega t)D(t) \ . \tag{3.20}$$

If a measurement of X is statistically significant in the sense given above but a measurement of Y is not, this may be regarded as evidence that there is no annual modulation in the background (except one satanically peaked in May or November).[16]

For illustration, in Figures 3 and 4 we show two typical data sets $D(t)$, binned into daily counts, generated at random by computer. In both cases the 'noise' term, $S_0(t) + B(t)$, was generated from a parent Poisson distribution with $\langle S_0 \rangle + \langle B \rangle = 10$ counts per day and variance equal to the mean. Figure 3 corresponds to pure noise, that is, $\langle R \rangle = S_m = 0$. In this run, the measured values were $d_{tot} = 3680$ total counts, $x = -0.95$, modulation significance $r = -0.11$, and orthogonal modulation significance $y/\sqrt{2d_{tot}} = -0.56$. Such data would rightly be considered a null result for modulation. On the other hand, Figure 4 was generated by the same noise plus a cosine modulation with $S_m = 160$ and $\langle R \rangle = 1.87$. For this run, the measured values were $d_{tot} = 3628$ total counts, $x = 190.6$, modulation significance $r = 2.24$, and orthogonal modulation $y/\sqrt{2d_{tot}} = -0.05$. In this case, although the modulation cannot be picked out from the data by eye (even if one filters out high frequencies by using longer bins), the modulation analysis strongly suggests the presence of the true signal.

4. Signal and Modulation Rates

We now apply the foregoing statistical analysis to the measurement of WIMP signal modulation. The expected value of the modulation significance is

$$\langle R \rangle = \frac{S_m}{\sqrt{2\langle D_{tot} \rangle}} \, . \tag{4.1}$$

In designing an experiment, one should aim to insure that a halo mass density of a given type of WIMP will generate a significant modulation measurement, say, $\langle R \rangle > 1.3$ (90% confidence level), in the proposed apparatus in a year. The WIMPs in question will be assumed to have an isotropic velocity independent cross section, which we parametrize by

$$\sigma = 5.2 \times 10^{-40} \mathrm{cm}^2 \frac{m_W M g(m_W, M)}{(\mathrm{GeV})^2} Q^2 \, , \tag{4.2}$$

where $g(m_W, M)$ is given by Eqn.(2.9). Here, Q is a parameter which depends on the detector nucleus and the WIMP identity, examples of which we discuss in the next section.

To evaluate the modulation significance R, we must first calculate the expected average daily signal $\langle S_0 \rangle$ from a halo density of WIMPs, per kilogram-day of detection, at a given energy threshold A^2 [see Equation (2.17)]. From equations (2.19) and (4.2), the time-averaged count rate is

$$\frac{\langle S_0 \rangle}{\mathrm{kg-day}} = \frac{I(\eta_0, \epsilon)}{\mathrm{kg}} = 0.32 g(m_W, M) Q^2 \gamma(A^2) \bar{v}_{270} \rho_{0.4} \, \frac{\mathrm{counts}}{\mathrm{kg-day}} \, , \tag{4.3}$$

where the halo velocity dispersion $\bar{v} = 270 \bar{v}_{270}$ km/sec [see Equation (2.5) and discussion following], the local halo density $\rho_{halo} = 0.4 \rho_{0.4}$ GeV/cm^3, and $\gamma(A^2)$ gives the signal at energy threshold A^2 as a fraction of its value at zero threshold (see Fig. 5).[17] Note that, for values of $A^2 \lesssim 7$, the effects of the galactic escape velocity on the WIMP distribution can be safely ignored (see Appendix I). For $A^2 \gtrsim 7$, the function $\gamma(A^2)$ should be replaced by $\bar{\gamma}(A^2)$, shown in Figure 6.

We now consider the modulation under two different assumptions about the background. First assume that the expected background rate is much greater than the time-average signal, $\langle B \rangle \gg \langle S_0 \rangle$, and is given in units of tens per kilogram per day, $\langle B \rangle / \mathrm{kg} = 10 B_{10} \mathrm{kg}^{-1}$. In this case, the modulation significance is proportional to the absolute modulation, and from equations (2.23) and (4.1) is given by

$$\langle R \rangle_B = 0.041 g Q^2 \beta(A^2) B_{10}^{-\frac{1}{2}} \left(\frac{M_{det}}{\mathrm{kg}} \frac{\tau}{\mathrm{yr}} \right)^{\frac{1}{2}} \rho_{0.4} \bar{v}_{270} \ , \tag{4.4}$$

where M_{det} is the detector mass, and τ is the duration of the experiment. The function β, shown in Figure 5, gives the absolute modulation of the signal at energy threshold A^2 as a fraction of its value at zero threshold [see equation (2.23)]. We note the important fact that, although the signal-to-noise ratio $\langle S_0 \rangle / \langle B \rangle$ is approximately independent of detector size and counting time, the modulation significance scales as the square root of the number of kg-years of detection. For reference, we also give here the absolute modulation expressed as a daily rate,

$$\frac{1}{(\mathrm{kg})} \left(\frac{\partial I}{\partial \eta} \right)_{\eta_0} \Delta\eta = \frac{S_m}{365(\mathrm{kg-day})} = 9.4 \times 10^{-3} g Q^2 \beta(A^2) \rho_{0.4} \bar{v}_{270} \frac{\mathrm{counts}}{\mathrm{kg-day}} \ . \tag{4.5}$$

Now consider the opposite limit: suppose that the background from other sources is small compared to the time averaged WIMP signal, $\langle B \rangle \ll \langle S_0 \rangle$. In this case, from equations (2.19), (2.23), and (4.1), one finds that

$$\langle R \rangle_S = 0.23 g^{\frac{1}{2}} Q \alpha(A^2) \left(\frac{M_{det}}{\mathrm{kg}} \frac{\tau}{\mathrm{yr}} \rho_{0.4} \bar{v}_{270} \right)^{\frac{1}{2}} \ , \tag{4.6}$$

where

$$\alpha(A^2) \equiv \frac{\beta}{\gamma^{\frac{1}{2}}} \ . \tag{4.7}$$

The function α is shown in Figure 5. Note that it retains a value of $\alpha \simeq 1.5$ over a fairly broad range. The effects of finite galactic escape velocity on the modulation

parameters α and β are shown in Figure 7. As we discuss in Appendix I, the escape velocity has negligible impact on the modulation for $A^2 \lesssim 7$.

We note here that the *theoretical* uncertainty in R is dominated by the uncertainty in the local halo density. Also, for cases in which the background and signal are comparable ($1/10 \lesssim (S_0/B) \lesssim 10$), one should use the exact expression for the modulation significance (used in generating the figures below),

$$\langle R \rangle = \frac{\langle R \rangle_S \langle R \rangle_B}{(\langle R \rangle_S^2 + \langle R \rangle_B^2)^{1/2}} \ . \tag{4.8}$$

Clearly, in designing optimal detectors, one would vary the mass of the detector nucleus M and the threshold energy ϵ (or equivalently A^2) to maximize the functions in Equations (4.3) - (4.6) over a wide range of WIMP masses. In practice, such a project will be limited by availability of materials and the technological difficulty of achieving low thresholds in large detectors. We discuss examples of detectors and event rates in the next section.

Although the discussion above is completely general, it has not exploited the fact that conventional ionization detectors, and possibly cryogenic detectors, have substantial energy resolution. For an energy-sensitive detector, the average daily count rate at nuclear recoil energy ΔE can be found from the derivative of Equation (4.3),

$$\frac{I(\eta_0, \epsilon, \Delta E)}{\text{kg}} = 1.19 Q^2 \left(\frac{m_W}{\text{GeV}}\right)^{-1} \left(-\frac{d\gamma}{dA^2}\right)_{A_0} \frac{\rho_{0.4}}{\bar{v}_{270}} \frac{\text{counts}}{\text{kg} - \text{day} - \text{keV}} \ , \tag{4.9}$$

where

$$A_0^2 = A^2 \left(\frac{\Delta E}{\epsilon}\right) = \frac{3 \Delta E}{g m_W \bar{v}^2} \ , \tag{4.10}$$

and A^2 is given by Eqn.(2.17). The function $-d\gamma/dA^2$ is shown in Figure 5; again, for velocities near the galactic escape velocity, i.e., for $A^2 \gtrsim 7$, the function $-d\bar{\gamma}/dA^2$, shown in Figure 6, should be used. Note that Eqn.(4.9) is the detection

rate per keV of *nuclear* recoil energy, which is about a factor 3-5 times the equivalent electron energy, depending on material and energy range.[4] Here and below, all energies and count rates will be expressed in terms of nuclear rather than electron depositions.

If the background has a different dependence on energy than the signal, resolution is useful in distinguishing the two. For example, the noise seen in ultralow background Ge double beta decay detectors appears to be only weakly energy dependent: current background rates in these experiments are of order .1-.3 per kg per keV per day above $O(40)$ keV (nuclear recoil energy). By contrast, Figure 5 shows the expected WIMP signal is strongly peaked at low energy. Thus, if low thresholds can be achieved, and *if* the background does not increase sharply at low energy, one might hope to see the dark matter peak.

What role does energy resolution play in the detection of modulation? As Figure 8 shows, modulation of the WIMP signal gives rise to a sinusoidal dependence not only of the total count rate but of the recoil energy spectrum as well. (Fig.8 also shows why the modulation is maximal for $A^2 \simeq 1$, for this yields the maximum difference in the energy-integrated signal between May and December.) In practice, the modulation in the energy spectrum will be difficult to detect, because the seasonal variation in the number of counts *per energy bin* is small unless the WIMP signal is very large. For our purposes, energy resolution is primarily useful in rejecting background in the following way. Once the threshold of an experiment is fixed, one can determine from Fig.5 the energy range, $\epsilon < \Delta E < \tilde{E}$, over which one must look to see the bulk (say, 90%) of the modulation for a range of WIMP masses. We then reject all counts in the energy range $\Delta E > \tilde{E}$ as due primarily to noise, and evaluate the modulation significance R using only the remaining low energy data. Note that this method of background rejection is independent of assumptions about background levels, and depends only on the expected signal level.

5. Particles and Detection Rates

In this section, we evaluate the modulation significance and expected event rates for a variety of WIMP halo candidates and detectors. We first discuss the scattering parameter Q of Equation (4.2). For the well-known cases, we simply compile the results for reference. For cases which are less familiar or in which the literature provides no consensus, we provide more discussion. As mentioned in the Introduction, WIMPs can be classified according to whether their interactions with nuclei are: a) coherent, i.e., nuclear spin-independent, or b) spin-dependent. We will discuss examples of each type.

5.1. COHERENT PARTICLES AND COSMIONS

For particles with spin-independent interactions, Q is roughly proportional to the atomic number of the nucleus, i.e., to the nuclear mass. For example, for Dirac neutrinos, neutral current interactions give

$$Q_{\nu_D} = N - (1 - 4\sin^2\theta_w)Z \simeq N - .12Z \ , \tag{5.1}$$

slightly less than the number of neutrons. (We are ignoring the small contribution due to the axial vector coupling, which is negligible for $Z \gtrsim 2$.) For scalar neutrinos, candidates for the lightest supersymmetric particle, $Q_{\tilde{\nu}} = 2Q_{\nu_D}$. From Eqn.(4.2), it follows that heavy target nuclei are preferred for detecting these particles.

Another class of 'coherent' cold dark matter candidates are cosmions, relatively light particles (3 GeV $\lesssim m_c \lesssim$ 7 GeV) with larger nuclear interaction cross-sections than the particles above, which are candidates to solve the solar neutrino problem.[18] As an example, we will consider one of the cosmions proposed by Gelmini, Hall, and Lin,[19] a Dirac fermion with a cosmic asymmetry, which interacts with light quarks via a heavy colored scalar, ϕ. The low energy

cross-section for cosmion-nucleus scattering is

$$\sigma_c = \frac{(N+2Z)^2}{4\pi}\frac{h^4}{m_\phi^4} m_c M g(m_c, M) \ , \tag{5.2}$$

where h is a Yukawa coupling constant, m_c is the cosmion mass, and m_ϕ is the mass of the exchanged heavy scalar. To solve the solar neutrino problem requires that the cosmion have an average scattering cross-section of $\simeq 2 - 10 \times 10^{-36}$ cm^2 per baryon in the sun[18]. If we fix the ratio $(h/m_\phi)^4 \simeq 4.6(m_c/\mathrm{GeV})^{-1}(100\mathrm{GeV})^{-4}$, then for cosmion masses of 3 GeV and 10 GeV, the cosmion-proton cross-sections are 4×10^{-36} cm^2 and 2×10^{-36} cm^2 respectively. Consequently, from Equation (4.2), the cosmion scattering parameter is approximately

$$Q_c \simeq 53(N+2Z)\left(\frac{m_c}{\mathrm{GeV}}\right)^{-\frac{1}{2}} \ . \tag{5.3}$$

In this example, the cosmion has coherent interactions with nuclei; we note than in other models, the cosmion may have only spin-dependent interactions.[19].

5.2. SPIN-DEPENDENT INTERACTIONS

Popular candidates for halo particles with spin-dependent nuclear interactions include three Majorana fermions: Majorana neutrinos, higgsinos and photinos. For Majorana neutrinos,[20]

$$Q^2_{\nu_M} = 20.5\lambda^2 J(J+1) \ , \tag{5.4}$$

where $\lambda^2 J(J+1)$ is a parameter which depends on the nucleus. Here and below, we have normalized our definitions of Q^2 so that the values of $\lambda^2 J(J+1)$ given by Goodman and Witten (ref.4) and Drukier, Freese and Spergel (ref.5) should be used, even in cases where our estimates for cross sections differ. The nuclear shell model parameter $\lambda^2 J(J+1)$ is only appreciable for nuclei with an odd number of protons or neutrons. For several favorable nuclei, $\lambda^2 J(J+1) = .5$ (^{7}Li, ^{11}B), 0.91 (^{19}F), .42 (^{27}Al), and 0.40 (^{51}V).

In supersymmetric theories, the lightest supersymmetric particle (LSP) may be a Majorana fermion, a partner to ordinary bosons. In general, the lowest mass eigenstate will be a mixture of the photino, higgsinos, and the zino. We will consider two limiting cases, in which the LSP is an almost pure higgsino or an almost pure photino. For higgsinos,

$$Q^2_{\tilde{H}} = Q^2_{\nu_M} \cos^2 2\alpha \ , \tag{5.5}$$

where $\tan\alpha = v_2/v_1$ is the ratio of the vacuum expectation values of the two Higgs doublets. The result in Eqn.(4.5) assumes higgsinos scatter predominantly through Z_0 (rather than squark) exchange, which holds provided α is not too close to $\pi/4$, i.e., for $\tan\alpha \neq 1$. Theoretical prejudice appears to favor $\tan\alpha < 1$.

For photinos, the nuclear scattering cross-sections are somewhat uncertain. The calculation proceeds in two steps: we first evaluate the cross-sections for scattering of photinos by protons and neutrons and then use the nuclear shell model to obtain photino-nucleus cross sections. Assuming all scalar quark masses $m_{\tilde{q}}$ are degenerate and negligible left-right squark mixing, the photino-nucleon cross section can be written[21] $(N = p, n)$

$$\sigma_{\tilde{\gamma}N} = \frac{3}{\pi}\left(\frac{4\pi\alpha}{m^2_{\tilde{q}}}\right)^2 \frac{m^2_{\tilde{\gamma}} m^2_N}{(m_{\tilde{\gamma}} + m_N)^2}\left(\sum_{q=u,d} e^2_q G^N_q\right)^2 \ , \tag{5.6}$$

where e_q is the quark electric charge. Here, G^N_q are the axial charges associated with the constituent quarks, defined by the matrix elements of the axial quark current for nucleon eigenstates,

$$\langle N, p', s'|\bar{q}\gamma_\mu\gamma_5 q|N, p, s\rangle = G^N_q \bar{u}_N(p', s')\gamma_\mu\gamma_5 u_N(p, s) \ , \tag{5.7}$$

where $p(p')$, $s(s')$ denote the initial (final) four momentum and spin of the nucleon. By decomposing the axial current into isosinglet and isovector parts, the

axial charges can be related to the vector and singlet coupling constants g_{A3} and g_{A0},

$$G_d^n = G_u^p = \frac{1}{2}(g_{A0} + g_{A3}) \ ,$$

$$G_u^n = G_d^p = \frac{1}{2}(g_{A0} - g_{A3}) \ . \tag{5.8}$$

The isovector coupling constant is measured to be $g_{A3} = 1.25$; unfortunately, the isosinglet coupling g_{A0} is not determined experimentally, so we will retain it as a parameter.

Putting these results together gives the cross-section for photinos on nucleons; multiplying by the shell model factor $1.1\lambda^2 J(J+1)$ (since $\lambda^2 J(J+1)_{p,n} = 0.91$) and using Eqn.(3.22) finally yields

$$Q_{\tilde{\gamma}}^2 = 271.5 \left(\frac{50\text{GeV}}{m_{\tilde{q}}}\right)^4 \lambda^2 J(J+1) \left[\frac{1}{2}\left(\frac{5}{9}g_{A0} \pm \frac{1.25}{3}\right)\right]^2 \ , \tag{5.9}$$

where the +(-) sign is for shells with an extra proton (neutron) or proton (neutron) hole. The five elements described above all have an extra proton or proton hole. In this expression, we have scaled the cross-section to that for a scalar quark mass of 50 GeV, the lower limit set by UA1 data.[22]

It is often assumed that the photino halo arises from a critical cosmological density of photinos, $\Omega_{\tilde{\gamma}} = 1$. However, this assumption depends upon unknown details of galaxy formation (e.g., biasing) and uncertainties in the amount of dark matter in galaxy halos. At this point, it is equally plausible that $\Omega_{\tilde{\gamma}} \simeq 0.2 - 0.6$, the range of values of recent measurements of the density parameter. If we further assume degeneracy between the lightest squark and slepton masses, a 'Lee-Weinberg' calculation implies an approximate relation between squark and photino masses[21] (for $m_{\tilde{\gamma}} \gtrsim 10$ GeV)

$$m_{\tilde{q}} = 56 \text{ GeV } (1 + 0.04 m_{\tilde{\gamma}}^2)^{1/4} \left(\frac{\Omega_{\tilde{\gamma}} h^2}{0.25}\right)^{1/4} \ , \tag{5.10}$$

where $m_{\tilde{\gamma}}$ is the photino mass in GeV, $h = H_0/100$ km/sec/Mpc is a measure

of the Hubble constant, and we have approximately scaled the results from the case $\Omega_{\tilde{\gamma}}h^2 = 1/4$ treated in ref.21. Given these assumptions, we can express the photino scattering parameter as

$$Q_{\tilde{\gamma}}^2 = \frac{43.2\lambda^2 J(J+1)}{(1+0.04m_{\tilde{\gamma}}^2)} \left(\frac{\Omega_{\tilde{\gamma}}h^2}{0.25}\right)^{-1} \left(\frac{5}{9}g_{A0} \pm 0.417\right)^2 . \tag{5.11}$$

Different values for the axial isosinglet coupling g_{A0} have been used in the literature. Goodman and Witten[4] use the quark model prediction $g_{A0} = 1$, while Srednicki, Olive and Silk[2] use the quark model relation $g_{A0} = (3/5)g_{A3} = 0.75$; Kane and Kani[21] use SU(3) flavor relations to obtain $g_{A0} = 0.45$. Although these values give differing cross sections, they all imply that nuclei with an extra proton are favored over those with an extra neutron for photino detection. Recently, however, the spin-dependent structure function of the proton was measured by the EMC collaboration at $q^2 = 3$ GeV^2, giving a value approximately half of that predicted by the quark model. If we assume the structure function does not have strong dependence on q^2, this may be interpreted[23] as implying a much smaller value for the isosinglet coupling, $g_{A0} \simeq 0.01$. In this case, aside from shell model factors, nuclei with an extra proton or an extra neutron would be roughly equally favorable for photino detection. For several nuclei with neutron or neutron holes, $\lambda^2 J(J+1) = 0.91$ (^{3}He, ^{29}Si), 0.5 (^{9}Be), and 0.37 (^{73}Ge).

5.3. Detection Rates

In this subsection, we apply the foregoing results to calculate detection and modulation rates for a variety of WIMPs in several detectors: germanium, silicon, boron and fluorine.

Germanium

Experiments to detect neutrinoless double beta decay using ultralow background Ge detectors have been operating for some time. Two groups[3] have used

these detectors to place an upper bound on the mass of coherently interacting halo WIMPs, $m_W \lesssim 20$ GeV. These detectors were operated at a threshold of 4 keV equivalent electron energy, corresponding to $\epsilon \simeq 17$ keV nuclear recoil threshold. Near the threshold, both detectors measured count rates $\simeq 2.5$ kg^{-1} keV^{-1} day^{-1} (nuclear recoil energy), dropping to $0.1 - 0.3$ kg^{-1} keV^{-1} day^{-1} at recoil energies above $O(40)$ keV (see Fig. 9). Recently, both the UCSB-LBL and USC-PNL collaborations have decreased their thresholds to 1.5 keV equivalent electron energy, or $\epsilon \simeq 7.5$ keV nuclear recoil, with detector masses of 1.8 and 2.3 kg respectively, and will be running in the near future.

In Figures $9 - 13$, we show the expected recoil energy spectra, absolute count rates and modulation significance in the upgraded Ge detectors for the coherently interacting particles discussed in section 5.1 above. Figs. 9, 11 and 12 show that the minimum mass WIMP detectable via direct measurement of the recoil spectrum depends sensitively on the background level near the threshold. For example, Fig. 9 shows that Dirac neutrinos of mass as low as 10 GeV can be detected with the recoil spectrum if the background near threshold is well below 1 per kg per keV per day. (In this figure, the vertical dotted line corresponds to the threshold in the upgraded version of the Ge detectors. The horizontal dotted line corresponds to a background rate of order 0.1 per kg per keV per day, which has been achieved in this detector at recoil energies above 40 keV.) On the other hand, if the background rate at the new threshold of 7.5 keV is of order 2-3 per kg per keV per day, *i.e.*, comparable to the background rate at the old threshold (boxed points in Fig. 9), then the minimum mass Dirac neutrino detectable through the recoil spectrum is increased to 12 GeV.

Fig. 10 shows the modulation significance for Dirac neutrinos for the upgraded UCSB-LBL detector (the numbers for the USC-PNL detector are slightly higher). We see that a 95% confidence level measurement of the modulation can be achieved in 1 year down to a neutrino mass of 8 GeV. Here, the total background has been estimated by integrating an assumed constant background rate of 0.2 per kg per keV per day from the threshold up to a cut-off energy

$\tilde{E}$ chosen such that 90% of the modulation signal is retained. Thus, if a signal is seen in the recoil spectrum, it can easily be confirmed via modulation in a year. Furthermore, even with the relatively low background level assumed here, modulation can be used to probe to a lower neutrino mass than can be seen with the recoil spectrum (8 GeV vs. 10 GeV). In addition, if the background level at low recoil energies is higher (as discussed above), the minimum neutrino mass detectable via modulation is only slightly increased, while the minimum mass detectable through the recoil spectrum rises more sharply with increasing background. Thus, for high background levels, modulation can be used as a method of direct detection of WIMPs.

For cosmion detection, Figs. 11 and 12 show that the detection rate and minimum detectable mass depend sensitively on the galactic escape velocity. In Fig. 11, where $v_{esc} = \infty$ is assumed, the rates are much higher than in Fig. 12, where a cut-off with $v_{esc} = 575$ km/sec is assumed. Thus, in detecting low mass WIMPs, it is important to include the effects of the galactic cut-off. If a cut-off of 575 km/sec is assumed (see Appendix I), the Ge detector can directly probe down to a cosmion mass of order 7 GeV, which is the approximate upper limit on the mass for effective heat transport in the sun.[18] A statistically significant modulation could be measured down to 6.6 GeV in a year for GHL cosmions with this detector.

Silicon

Recently, a proposal to build a 500 gm conventional Silicon detector[24] with a threshold of $\epsilon = 1.8$ keV nuclear recoil has been made, in order to test the solar cosmion hypothesis. Compared to germanium, this detector has the advantage that its lower nuclear mass allows low mass WIMPs to be more easily detected (for a given threshold). In addition, silicon appears to be more efficient as a detector of nuclear recoil.

Figures 14-17 show expected event rates in this detector for Dirac neutrinos and GHL cosmions. Again, for Dirac neutrinos, the minimum detectable mass

(via the recoil spectrum) depends crucially on the background rate at low energy. As the noise level is increased from 0.5 to 5 counts per keV per kg per day, the minimum mass rises from 3.5 to approximately 9 GeV. As Figure 15 shows, for a 95% confidence level modulation measurement in 1 year, the minimum mass rises much more slowly as background levels increase over the same range, from 3.5 GeV to 5 GeV. Thus, for large background levels, modulation can be used to detect or rule out Dirac neutrinos down to lower masses than can be achieved with the direct signal, in fact, down to masses for which the signal-to-noise ratio is well below 1. Figures 16 and 17 show that GHL cosmions in the mass range of interest, 3-7 GeV, can be easily detected, and their modulation easily measured, with a Si detector operating for a year. In this case, signal levels are so high that modulation of the recoil spectrum (Fig.8) should be measurable; this would be a valuable probe of the halo distribution function.

Unfortunately, the isotope of silicon useful for detecting particles with spin-dependent interactions, ^{29}Si, has a natural abundance of only 4.7%. Thus, unless a large mass of pure ^{29}Si can be made, this detector will not be useful for finding Majorana fermions.

Boron and Fluorine

As mentioned in Section 5.2, two odd nuclei well-suited to detection of spin-dependent particles are ^{9}B and ^{19}F. In Figures 18-22, we show expected daily event rates and yearly modulation significance for Majorana neutrinos and photinos, assuming 2 kg detectors of boron and fluorine. In all cases, a background level of 0.5 per kg per day was assumed.

First consider Majorana neutrinos. Figs. 18 and 21 show that a 90% confidence level measurement of the modulation can be achieved in a year over a wide range of WIMP masses, e.g., $5 - 70$ GeV for fluorine, at a moderate threshold of order 3 keV. Note that, for fluorine, at the lower end of this mass range, the the signal-to-noise ratio is only of order 1 and at the upper end it is of order 6.6. This demonstrates once again the possibility of measuring the modulation

at low signal-to-background levels. More to the point, this can be achieved at thresholds above 1 keV, which appears to be accessible to conventional detectors. Although the signal can be increased by going to sub-keV thresholds, recall that the modulation significance is optimized at $A^2 \simeq 2$, which corresponds to a fluorine threshold of 3 keV for a WIMP mass of 7 GeV. Except at the very lowest masses, and modulo considerations of the detector efficiency of different materials, fluorine appears to be a better choice for Majorana neutrino detection than boron. We also note that the signal rate for higgsinos can be obtained from Figs.18 and 21 by multiplying by the factor $\cos^2 2\alpha$ [Eqn.(5.5)]. The modulation significance $\langle R \rangle$ for higgsinos is obtained from the Majorana neutrino significance by multiplying by a factor between $\cos^2 2\alpha$ (for background larger than signal) and $\cos 2\alpha$ (for signal larger than background).

For photinos, the scattering rate was calculated using Eqn.(5.11), with isosinglet coupling $g_{A0} = 0.45$, for two different cosmological photino densities (assuming fixed halo density): $\Omega_{\tilde{\gamma}} = 1$, $h = 0.5$ (dotted curves) and $\Omega_{\tilde{\gamma}} = 0.2$, $h = 0.5$ (dashed curves). If the value for g_{A0} inferred from the recent EMC data proves correct, the photino signal rate will be approximately a factor 2.5 smaller than that assumed here; the modulation significance will fall by a factor between 1.6 (for signal larger than background) and 2.5 (for background larger than signal). [On the other hand, if the quark model prediction $g_{A0} = 0.75$ is used, the photino signal will be a factor 1.56 larger than that shown here, and $\langle R \rangle$ will increase by a factor between 1.2 (for $S_0 \gg B$) and 1.56 (for $S_0 \ll B$)]. Figure 22 shows that 90% C.L. photino detection in a year is feasible with a 2 kg fluorine detector and 2 keV threshold for a photino mass below 15 GeV, assuming a low cosmological photino density. Figures 19 and 20 give the corresponding rates for photinos on boron for two different values of the threshold. This comparison shows again that the signal rate can be significantly improved by lowering the threshold, but that the modulation is optimized at moderate threshold, above 1 keV. In these figures, we have only shown photino masses larger than 7 GeV, for which Eqn.(5.10) is a reasonable approximation. In addition, for smaller photino

masses, the 'Lee Weinberg' value of the squark mass [Eqn. (5.10)] approaches the experimental lower bound[22] of 50 GeV. Thus, for low mass photinos, 3 GeV $\lesssim m_{\tilde{\gamma}} \lesssim$ 7 GeV, one can estimate the photino scattering rate using Eqn. (5.9) instead of (5.11). In this mass range, for a fixed squark mass of 50 GeV, the photino detection rate can be inferred from the Majorana neutrino rate using the relation $Q^2_{\tilde{\gamma}}(m_{\tilde{q}} = 50\text{GeV}) = 1.47 Q^2_{\nu_M}$.

6. Conclusion

We have presented a general analytic discussion of WIMP detection, applicable to a wide variety of cold dark matter candidates and particle detectors. Our principal analytic results are shown in Section IV. The reader can use these results to instantly calculate event rates for his or her favorite WIMP by using the following simple procedure. First, select the detector (nuclear mass M) and threshold energy ϵ. Use Fig. 1 to insure that the coherence loss parameter $b \ll 1$ for the WIMP mass range of interest; if not, choose a detector with lighter nuclei. Second, use Eqn. (2.17) or Fig. 2 to find the threshold parameter A^2 for a given WIMP mass, and use this to read out the signal and modulation parameters α, β, γ and $-d\gamma/dA^2$ from Figs. 5, 6, or 7. Third, use Eqn. (4.2) to find the value of the scattering parameter Q^2, and use Eqn. (2.9) to calculate $g(m_W, M)$. Finally, use Eqns. (4.3)-(4.9) to calculate the signal rate, the recoil spectrum, and the modulation significance for different assumptions about the background rate.

We have made a careful study of expected event rates in several detectors, including threshold effects and the galactic escape velocity. We have investigated the conditions for the modulation of the WIMP signal to be statistically significant, and have demonstrated the use of modulation as a primary means of WIMP detection at low signal-to-noise levels. In particular, this implies that modulation can be used to probe to smaller WIMP masses than the recoil energy

spectrum. For most particles and detectors, the modulation significance is optimized at moderate thresholds, possibly accessible to conventional detectors. For example, a 2 kg detector of ^{19}F with a threshold of 3 keV operating for a year can detect the otherwise elusive Majorana fermions (Majorana neutrinos, photinos, higgsinos) at the $90 - 95\%$ confidence level over a wide range of masses. Thus, we believe that many of the proposed halo WIMP candidates can be detected with devices which could be implemented in the near future.

Acknowledgements:

For useful conversations, we thank Frank Avignone, Stan Brodsky, David Caldwell, Andrjez Drukier, Mark Goodman, Howie Haber, Vicki Lindsay, Sterl Phinney, Joel Primack, Bernard Sadoulet, Mark Srednicki, Gary Steigman and Mike Witherell. This work was supported by DOE contract DE-AC03-76F00515 at SLAC and by NSF under Grant. No. PHY82-17853, supplemented by funds from NASA at Santa Barbara.

APPENDIX I. Modulation and the Galactic Escape Velocity

In the body of the paper we assume that the WIMP speed distribution is Maxwellian, but in reality the distribution will be cut off at the local galactic escape velocity. Here we wish to show that our approximation introduces no significant errors in the evaluation of the signal modulation, unless the threshold is very high. One way to do this is to consider Figure 7, where we show the modulation function $\alpha(A^2)$, calculated with $v_{esc} = \infty$, compared with the function $\bar{\alpha}$, for which a cut-off at 575 km/sec was assumed (see discussion below). For $A^2 \lesssim 11$, there is a negligible difference in the results. However, this can also be understood analytically.

Let the WIMP distribution in the (non-rotating) galactic rest frame, f_0^{cut},

be cut off at the escape velocity[25] v_{esc},

$$f_0^{cut}(v) = f_0(v)\ \theta(v_{esc} - v)\ , \tag{I.1}$$

where $f_0(v)$ is the Gaussian distribution given by Equation (2.2). By the same galilean transformation as before, one finds the truncated distribution in the earth's frame

$$f_\eta^{cut}(x) = f_\eta(x)\ , \qquad x < \rho - \eta \tag{I.2}$$

$$f_\eta^{cut}(x) = \frac{n_W x}{\pi^{\frac{1}{2}}\eta}\left\{\exp[-(x-\eta)^2] - \exp\left[-\left(x + \left(\frac{\rho^2 - x^2 - \eta^2}{2x}\right)\right)^2\right]\right\}, \ \rho - \eta < x < \rho + \eta \tag{I.3}$$

where $f_\eta(x)$ is the untruncated distribution given by (2.3), x and η are defined in (2.4), and the parameter ρ is the dimensionless escape speed,

$$\rho^2 = \frac{3v_{esc}^2}{2\bar{v}^2}\ . \tag{I.4}$$

At $x = \rho$, i.e., for particles moving at the escape velocity *relative to the earth*, the ratio of the cut-off to the non-truncated distribution is

$$\frac{f_\eta^{cut}(\rho)}{f_\eta(\rho)} = \frac{e^{-(\rho-\eta)^2} - e^{-(\rho-\eta^2/2\rho)^2)}}{e^{-(\rho-\eta)^2} - e^{-(\rho+\eta)^2}} \simeq 1 - \exp(-2\rho\eta + 2\eta^2 - \frac{\eta^4}{4\rho^2}) \tag{I.5}$$

The local galactic escape velocity is not well determined, but studies of high proper motion stars indicate $v_{esc} > 500$ km/sec.[26] Assuming the galaxy has a flat rotation curve extending from r_0, the solar galactocentric distance, to a cut-off radius r_{lim}, the local escape velocity can be inferred from the local circular speed[26] (see discussion following Eqn.(2.5)),

$$\left(\frac{v_{esc}}{v_{circ}}\right)^2 = 2\ \ln\left(\frac{r_{lim}}{r_0}\right) + 2\ . \tag{I.6}$$

Using $r_0 \simeq 9$ kpc and assuming $r_{lim} \simeq 100$ kpc yields $v_{esc} = 575 \pm 50$ km/sec. (The probable error quoted here is due solely to the uncertainty in the circular

speed.) The central value of this estimate corresponds to $\rho = 2.6$. Evaluating (I.5) at this value and using $\eta_0 = 1.05$ yields $(f_\eta^{cut}/f_\eta)_{x=\rho} = 0.96$. Thus, the flux at the cut-off velocity, in the earth's frame, is very close to its value in the non-cut-off case. The reason for this is that most of the particles moving at 575 km/sec in the earth's frame come from the densely populated region of phase space near 340 km/sec ($x \simeq \rho - \eta$) in the galaxy frame, not from the high velocity tail. In the non-cut-off case, the contribution to the flux at $x = \rho$ from particles above the escape velocity is exponentially suppressed. This is not surprising, since less than 1% of the particles in a Gaussian distribution are above the virial escape velocity. Thus, as Equation (2.3) suggests, modulation arises principally from the sensitive velocity dependence of the WIMP distribution function, not from the cut-off. (Alternatively, for a flatter distribution function, modulation would be more sensitive to the escape velocity.)

To demonstrate this concretely, we evaluate the logarithmic derivative of Equation (I.5); using the values of the parameters given above yields

$$\frac{1}{f_\eta^{cut}(\rho)}\frac{df_\eta^{cut}(\rho)}{d\eta} - \frac{1}{f_\eta(\rho)}\frac{df_\eta(\rho)}{d\eta} \simeq 0.04 \ . \tag{I.7}$$

This shows that the cut-off has little effect on the sensitivity of the distribution function to a small change in η. But it is precisely this sensitivity which gives rise to the modulation. (Recall that the relative modulation is given by $(dI/d\eta)(\Delta\eta/I)$ and $I \sim f_\eta$.) On the other hand, if the detector threshold is set very high, so that the dimensionless threshold energy $A^2 \equiv x_{min}^2 \gtrsim \rho^2$, the detector will sample all corresponding incoming WIMP velocities *above* this value. Since, according to equation (I.3), the cut-off distribution goes smoothly to zero as $x \to \rho + \eta$, while the non-cut-off distribution remains finite, the logarithmic derivative (I.7) will clearly be larger at these higher velocities (i.e., at $x > \rho$). Thus, one might expect the cut-off to have a large impact on the modulation at this high threshold. However, for $x \to \rho + \eta$, the non-cut-off distribution is also highly Boltzmann-suppressed, so that inclusion of this region does not qualitatively change our conclusions. That is, the detector will mainly be sensitive to

WIMPs with energies very near the threshold, $x \simeq x_{min} = \rho$, where the effect of the cut-off is small.

In Figures 6 and 7, we show the count rate and modulation modified to include the effects of the cut-off at the escape velocity. In Fig.6, the function $\gamma(A^2)$ defined above, which is relevant for $v_{esc} = \infty$, is compared with the corresponding function $\bar{\gamma}(A^2)$, the relative count rate for $v_{esc} = 575$ km/sec. Similarly, in Fig.7, the corresponding modulation functions are compared in the cut-off and non-cut-off cases. [The functions $\bar{\gamma}$, $\bar{\alpha}$, and $\bar{\beta}$ are obtained by using equations (I.2) and (I.3) in equation (2.1), in place of (2.3).] For $A^2 \simeq 8$, the count rates (γ and $\bar{\gamma}$) differ by $O(30\%)$, while for $A^2 \simeq 12$ the rate is reduced by an order of magnitude in the cut-off case. Note that, with the cut-off, the count rate is strictly zero for $A^2 > (\rho + \eta)^2 = 13.3$.

APPENDIX II. Modulation and Loss Of Coherence

For Dirac neutrinos, scalar neutrinos, or other WIMPs with coherent nuclear interactions, the signal is greatly enhanced by using detectors composed of heavy nuclei [see Equations (5.1), (5.3)]. However, if the WIMP mass is also large, one finds from equation (2.16) that the coherence loss parameter b is no longer negligibly small (see Figure 1). In this case the detection integral, (2.1), must be done using the general expression for the scattering parameter, Equation (2.15), rather than (2.18). Then, for the detection rate, equation (2.19) is replaced by

$$I(\eta, \epsilon) = \left(\frac{8}{3\pi}\right)^{\frac{1}{2}} \frac{\sigma N n_w \bar{v}}{2\eta b} \left[e^{-bA^2} \chi(A_-, A_+) - \frac{\exp(-\frac{b}{1+b}\eta^2)}{(1+b)^{\frac{1}{2}}} \chi(\check{A}_-, \check{A}_+) \right] \quad \text{(II.1)}$$

where

$$A_\pm = A \pm \eta, \qquad \check{A}_\pm = A(1+b)^{\frac{1}{2}} \pm \frac{\eta}{(1+b)^{\frac{1}{2}}} \quad \text{(II.2)}$$

Figure 23 shows the modulation function $\alpha(A^2)$ for a range of values of $b = 0.0, 0.1, ..., 1.0$. We see that, for large values of $b \sim 1$, i.e., if the loss of coherence

is significant, the modulation may be severely reduced or eliminated at both large and small thresholds, and may even reverse its sign. The explanation for this reduction is straightforward: when the earth is moving faster through the halo in May, the average momentum transfer between WIMPs and detector nuclei is increased. From Equation (2.10), this leads to a greater reduction in the signal due to loss of coherence than at other times of the year, so the net modulation is decreased.

For most cases of interest, this potential loss of coherence and modulation is not important for detector design. For example, consider a Dirac neutrino with a mass of 20 GeV, the upper limit set by Ge double beta decay experiments. For the germanium detectors now in operation, the coherence loss parameter is $b = 0.07$. For the recently upgraded detectors, the threshold is $\epsilon \simeq 7.5$ keV, corresponding to $A^2 \simeq 1.9$. From Figure 23, we see that the expected modulation significance $\langle R \rangle$ is reduced by $\simeq 14\%$ (assuming signal much larger than background). However, as Figure 9 shows, the expected value of $\langle R \rangle$ for 1.8 kg of Ge and a 20 GeV Dirac neutrino is 17.2 for 1 year, not corrected for the effects of coherence loss. In this case, coherence loss leads to a small reduction in the magnitude of the modulation and thus to a small adjustment in the analysis of an experiment, but it would not be great enough to affect the design of the detector.

If the WIMP mass is above 20 GeV, the Ge detector bounds on the scattering cross-section suggest that such a particle has only spin-dependent interactions with nuclei. In this case, if the WIMP mass is not very large (which seems likely from cosmological abundance arguments), lighter detector nuclei will be preferred, and coherence loss is not a problem. Of course, one is free to imagine a very massive WIMP candidate with small but coherent nuclear interactions (say, with $Q^2 \simeq 10^{-2}N^2$), for which coherence loss would be a serious difficulty. However, such particles do not seem theoretically well motivated at the present.

REFERENCES

1. For an introductory review, see, e.g., J.R. Primack, lectures given at the International School of Physics, Enrico Fermi, Varenna, Italy, 1984.

2. J. Silk, K.A. Olive and M. Srednicki, Phys. Rev. Lett. 55, 257 (1985). M. Srednicki, K.A. Olive and J. Silk, Nucl. Phys. B279, 804 (1987). L. Krauss, K. Freese, W. Press and D. Spergel, Astrophys. J. 299, 1001 (1985). K. Freese, Phys. Lett.167B, 295 (1986). L. Krauss, M. Srednicki and F. Wilczek, Phys. Rev.D33, 2079 (1986). T. Gaisser, G. Steigman and S. Tilav, Phys. Rev. D34, 2221, (1986). K. Greist and D. Seckel, Nucl. Phys. B283, 681 (1987). K. Ng, K. Olive and M. Srednicki, Phys. Lett. 188B, 138 (1987). A. Gould, Astophys. J. (1987), in press. IMB collaboration preprint, 1986. Kamiokande collaboration preprint, 1987.

3. F.T. Avignone, III, etal., talk presented at the Int. Symp. on Weak and Electromagnetic Interactions in Nuclei, Heidelberg, West Germany, July 1986. S.P. Ahlen, etal., Harvard CfA preprint, 1986. D.O. Caldwell, in "Neutrino Masses and Neutrino Astrophysics", Proc. of Telemark IV conference, eds. V. Barger, etal. (World Scientific, 1987), p.262. D. O. Caldwell, etal., in preparation.

4. M. Goodman and E. Witten, Phys. Rev. D31, 3059 (1985). I. Wasserman, Phys. Rev. D33, 2071 (1986). A. Drukier and L. Stodolsky, Phys. Rev. D30, 2295 (1984). A. Drukier, Acta Physica Polonica, B17, 229 (1986). B. Cabrera, L. Krauss and F. Wilczek, Phys. Rev. Lett. 55, 25 (1985). B. Cabrera, D. Caldwell and B. Sadoulet, Proc. of 1986 Summer Study on Physics of the Superconducting Super Collider, Snowmass, CO, July, 1986. B. Sadoulet, J. Rich, M. Spiro and D. O. Caldwell, U.C. Berkeley preprint, October, 1986. A. Drukier and K. Freese, in preparation. For a review, see P. Smith, preprint RAL-86-029.

5. A. Drukier, K. Freese and D. Spergel, Phys. Rev. D33, 3495 (1986).

6. We should mention that modulation is not the *only* means for distinguishing a WIMP signal from background. For example, varying the atomic weight of the target will yield information about the mass and identity of the incident particles. In addition, bolometric detectors may have sufficient spatial and energy resolution to help distinguish a signal from radioactive backgrounds. See refs.4,5.

7. D. Lynden-Bell, Mon. Not. R. Astr. Soc. 136, 101 (1967). F. Shu, Astrophys. J. 225, 83 (1978).

8. J. Caldwell and J.P. Ostriker, Astrophys. J. 251, 61 (1981). Similar estimates of the local halo density were obtained by J. Bahcall and R. M. Soneira, Astrophys. J. Suppl. 44, 73 (1980). J. Bahcall, M. Schmidt and R. M. Soneira, Astrophys. J. 265, 730 (1983). These models assume an isothermal halo with a scale height $a \simeq 4 - 5$ kpc. We assume throughout that the halo density is due solely to WIMPs.

9. Joel Primack, private communication. G. R. Blumenthal, in "Nearly Normal Galaxies", Proc. of Santa Cruz conference, 1986. For earlier discussions of halo infall, see B.S. Ryden and J.E. Gunn, in "Dark Matter in the Universe", Proc. of IAU Symp.117, Princeton, 1985, eds. J. Kormendy and G.R. Knapp; G.R. Blumenthal, S.M. Faber, R. Flores and J.R. Primack, Astrophys. J. 301, 27 (1986). It appears that halo infall will enhance the distribution in the radial direction; according to ref.5, this increases the modulation rate. Thus, in terms of detecting modulation, the isotropic Gaussian distribution is very probably a 'worst case' scenario in comparison to more realistic models.

10. A. Gould, Astrophys. J., (1987), in press. Note that we are neglecting the effects of the solar and earth gravitational fields on the WIMP distribution. Since we are concerned in this paper with WIMPs of initial kinetic energy much higher than their gravitational potential energy, this approximation is justified.

11. This value is taken from the recent compilation by F. J. Kerr and D. Lynden-Bell, Mon. Not. Roy. Astr. Soc. 221, 1023 (1986) and references therein. For an earlier discussion, see D. Mihalas and J. Binney, *Galactic Astronomy*, (W.H. Freeman, San Francisco, 1981).

12. See, for example, K. Lang, *Astophysical Formulae*, (Springer-Verlag, Berlin, 1980).

13. See ref. 10. Note that it is only for coherently interacting WIMPs that very massive nuclei are desirable and thus coherence loss must be considered. For particles with only spin-dependent interactions, on the other hand, the most desirable detector nuclei are those that maximize energy loss, i.e., which match nuclear and WIMP masses. In this case, relatively small nuclear masses are desirable.

14. G. Eder, *Nuclear Forces: Introduction to Theoretical Nuclear Physics*, (M.I.T. press, Cambridge, 1968).

15. See, for example, J. D. Scargle, Astrophys. J. 263, 835 (1982).

16. We note that the solar neutrino signal will show an annual modulation due to the ellipticity of the earth's orbit, but the expected count rates are negligible (far below 1 per kg-day) compared to the halo WIMP signal. See ref.4.

17. We note that in Eqns.(4.3), (4.4), and (4.6) there is a more complicated but slight dependence on the halo and solar velocities which we have not displayed. Also note that in these equations, the approximate relation $M = 0.931(Z + N)$ GeV between nuclear mass and atomic number has been used. In the Figures, the exact nuclear masses are used.

18. D. N. Spergel and W. H. Press, Astrophys. J. 294, 663 (1985). W. H. Press and D. N. Spergel, *ibid.*296, 679 (1985). G. Steigman, C. Sarazin, H. Quintana and J. Faulkner, Astron. J. 83, 1050 (1978). M. Nauenberg, University of California, Santa Cruz preprint, 1986.

19. G. B.Gelmini, L. J. Hall and M. J. Lin, Nucl. Phys. B281, 726 (1987). For an alternative cosmion model, see S. Raby and G. West, Los Alamos preprints, 1987.

20. See, e.g., M. Srednicki, K. Olive and J. Silk, ref.2

21. This calculation was first carried out schematically by M. Goodman and E. Witten, ref.4. Our discussion here follows that of Srednicki, Olive and Silk, ref.2, and G. Kane and I. Kani, Nucl. Phys. B277, 525 (1986). We note that in models with significant mixing between left and right handed squarks, photinos would have coherent interactions with nuclei.

22. S. P. Geer (UA1 Collaboration), talk presented at Uppsala Conference, 1987. C. J. Seez (UA1 Collaboration), talk presented at the 2nd Topical Seminar on Heavy Flavor Physics, San Miniato, Italy, May 1987.

23. EMC Collaboration, talk presented at Uppsala Conference, 1987. J. Ellis, talk presented at Uppsala Conference, 1987. We thank Howie Haber for bringing this reference to our attention.

24. B. Sadoulet, etal., ref.4

25. In actuality, the distribution function will not be truncated discontinuously, but will instead go smoothly to zero as the escape velocity is approached. See, for example, I. R. King, Astron. J. 70, 376 (1965). However, for our purposes, the distribution (I.1) is an excellent approximation to a King model.

26. B. W. Carney and D. W. Latham, in "Dark Matter in the Universe", Proc. of IAU Symp. No.117, eds. J. Kormendy and G. Knapp (Reidel, Dordrecht, 1987).

FIGURE CAPTIONS

1) Coherence loss parameter b (Eqns.(2.14), (2.16)) as a function of target nucleus mass M, shown for a variety of WIMP masses m_W. For $b \ll 1$, the loss of coherence has a negligible effect on event rates.

2) Dimensionless threshold energy A^2 (Eqns.(2.14), (2.17)) as a function of target nucleus mass M, shown for a variety of WIMP masses m_W.

3) Sample data set for 1 year, showing the daily count rate $D(t)$. The data were generated from Poisson noise with a mean of 10 counts per day. The expected modulation significance $\langle R \rangle = 0$ and the measured value for this run is $r = -0.11$.

4) Same as Figure 3, but with an added cosine modulation $S_m = 160$, peaked at days 0 and 365. The expected modulation significance $\langle R \rangle = 1.87$ and the measured value for this run is $r = 2.24$.

5) Dimensionless measures of the WIMP signal (γ), the signal per unit energy ($-d\gamma/dA^2$), and the modulation significance when the signal is much greater than (α), or much less than (β) the background. These functions are plotted against the dimensionless threshold energy A^2. For definitions, see discussion following Eqn.(2.23) and also Eqns.(3.23-3.28).

6) Dimensionless measure of the WIMP signal shown for two halo models: an isothermal Maxwell-Boltzmann distribution with infinite escape velocity (γ, dotted curve), and a Maxwell distribution truncated at an escape velocity of 575 km/sec ($\bar{\gamma}$, solid curve). Also shown is the signal per unit energy in the truncated model ($-d\bar{\gamma}/dA^2$, dashed curve).

7) Same as Fig.6, for the modulation parameters α and β.

8) Modulation of the recoil energy spectrum.

9) Counts per energy bin as a function of nuclear recoil energy ΔE for germanium detector, shown for Dirac neutrinos of mass $m_W = 10$, 15 and

20 GeV. The horizontal dotted line corresponds to a background rate of order 0.1 per kg per keV per day, which has been achieved in this detector at recoil energies above 40 keV. The two boxed points correspond to data points (presumably noise) measured in the UCSB-LBL double beta decay detector before its recent upgrading. Similar count rates have been recorded in the USC-PNL detector. The vertical dotted line corresponds to the approximate threshold in the upgraded versions of these detectors.

10) Modulation significance for Dirac neutrinos for 1.8 kg-years of germanium, assuming a threshold energy $\epsilon = 7.5$ keV. Shown are the expected signal count rate in units of 10 per day, the modulation significance $\langle R \rangle$ and the 95% confidence level $R = 1.64$, the dimensionless threshold energy A^2, and the expected number of background counts per day, assuming a background rate of 0.2/(kg-keV-day) (nuclear recoil energy). This corresponds to 1 year of running the upgraded UCSB-LBL detector. For the upgraded USC-PNL detector, $M_{det} = 2.3$ kg, the signal and background per day should be scaled up by a factor 1.28 and the modulation significance by approximately 1.13. For scalar neutrinos, the signal should be scaled up by a factor 4 and the modulation significance by roughly 2. Note that this figure assumes $v_{esc} = \infty$. For the reduction in the modulation at large A^2 due to finite v_{esc}, see Fig.7.

11) Counts per energy bin for Ge detector, for GHL cosmions of mass $m_W =$ 6, 8, 10 GeV, assuming no cut-off for the halo distribution ($v_{esc} = \infty$). Also shown is the dimensionless energy parameter A_0^2 (Eqn.(4.10)) for each cosmion mass, as a function of the nuclear recoil energy. For $A_0^2 \gtrsim 8$, the rates shown here are significantly higher than the corresponding rates with a cut-off of $v_{esc} = 575$ km/sec imposed (Fig. 12). Vertical dotted line shows threshold for upgraded detectors.

12) Same as Figure 11, for cosmion masses 7,8 and 10 GeV, assuming a local galactic escape velocity of 575 km/sec. Note the reduction in count rate

and the steepening of the recoil spectrum due to the cut-off.

13) Modulation significance for GHL cosmions for 1.8 kg-years of germanium. The signal count rate is shown in units of 1000 per day and the modulation significance in units of 10. In this Figure, the halo distribution was not cut-off.

14) Recoil energy spectrum for Si detector, for Dirac neutrinos of mass 3.5, 5 and 10 GeV. Vertical dotted line corresponds to the proposed threshold of 1.8 keV (nuclear recoil). Also shown are two constant background rates: 0.5 counts/(kg-keV-day) (dotted) and 5 cts./(kg-keV-day) (dotdash).

15) Modulation significance for Dirac neutrinos with 500 gm-years Si detector with threshold of 1.8 keV. Shown are the signal in units of 10 per day and $\langle R \rangle$ for the two background rates shown in Figure 14.

16) Recoil energy spectrum in Si detector for GHL cosmions of mass 3.5, 5 and 7 GeV, with same background rates as in Fig. 14.

17) Modulation significance and signal for GHL cosmions in the proposed 500 gm Si detector, for 1 year of data.

18) Majorana neutrino detection rate and modulation significance for 2 kg ^{11}B detector with 2.5 keV threshold.

19) Photino detection rate for 2 kg boron detector with 2.5 keV threshold, assuming Eqn.(5.11) for the scattering parameter and axial coupling $g_{A0} = 0.45$. Dashed curves correspond to $\Omega_{\tilde{\gamma}} = 0.2$, $h = 0.5$, dotted curves to $\Omega_{\tilde{\gamma}} = 1$, $h = 0.5$. Here $h = H_0/100$ km/sec/Mpc.

20) Same as Fig.19, but with threshold 200 eV. Although the signal is significantly enhanced at the lower threshold, the modulation significance is reduced.

21) Majorana neutrino rate and modulation significance for ^{19}F detector with 3 keV threshold.

22) Same as Fig.19 for the fluorine detector.

23) Modulation parameter $\alpha(A^2)$ for various choices of the coherence loss parameter b.

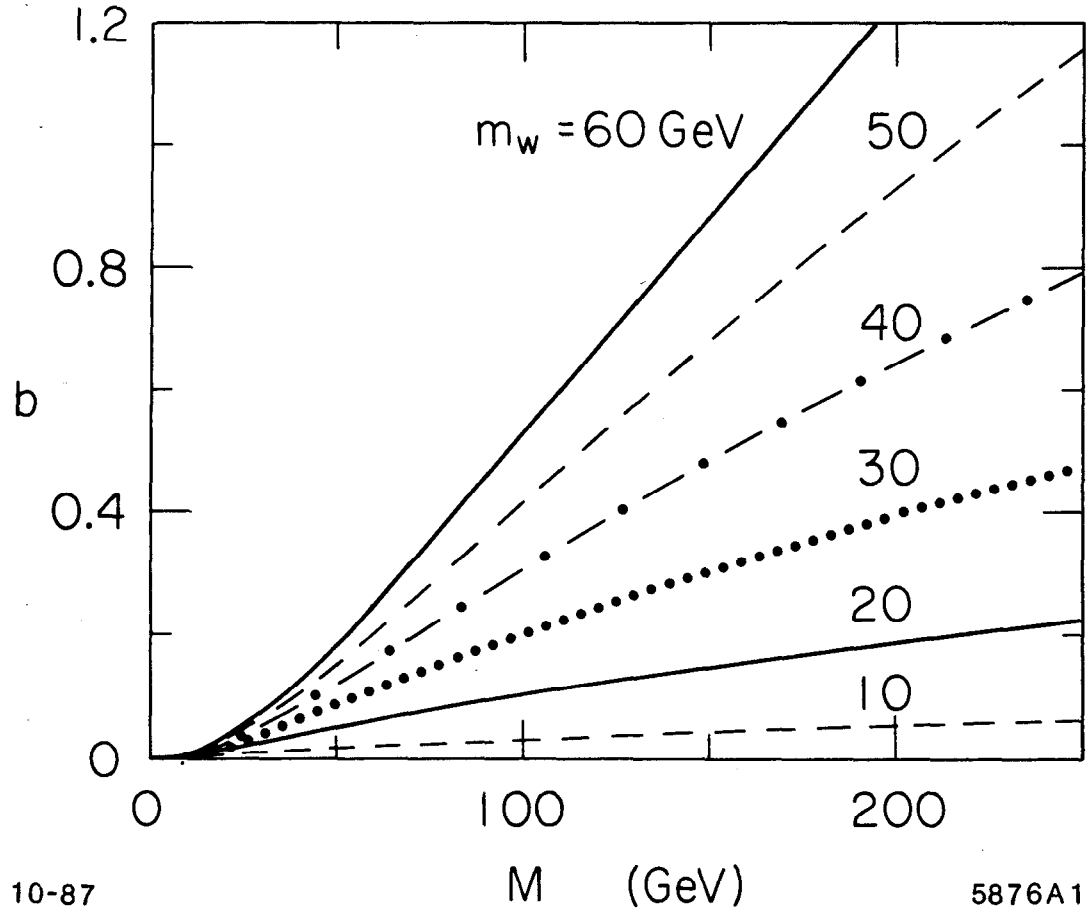

Fig. 1

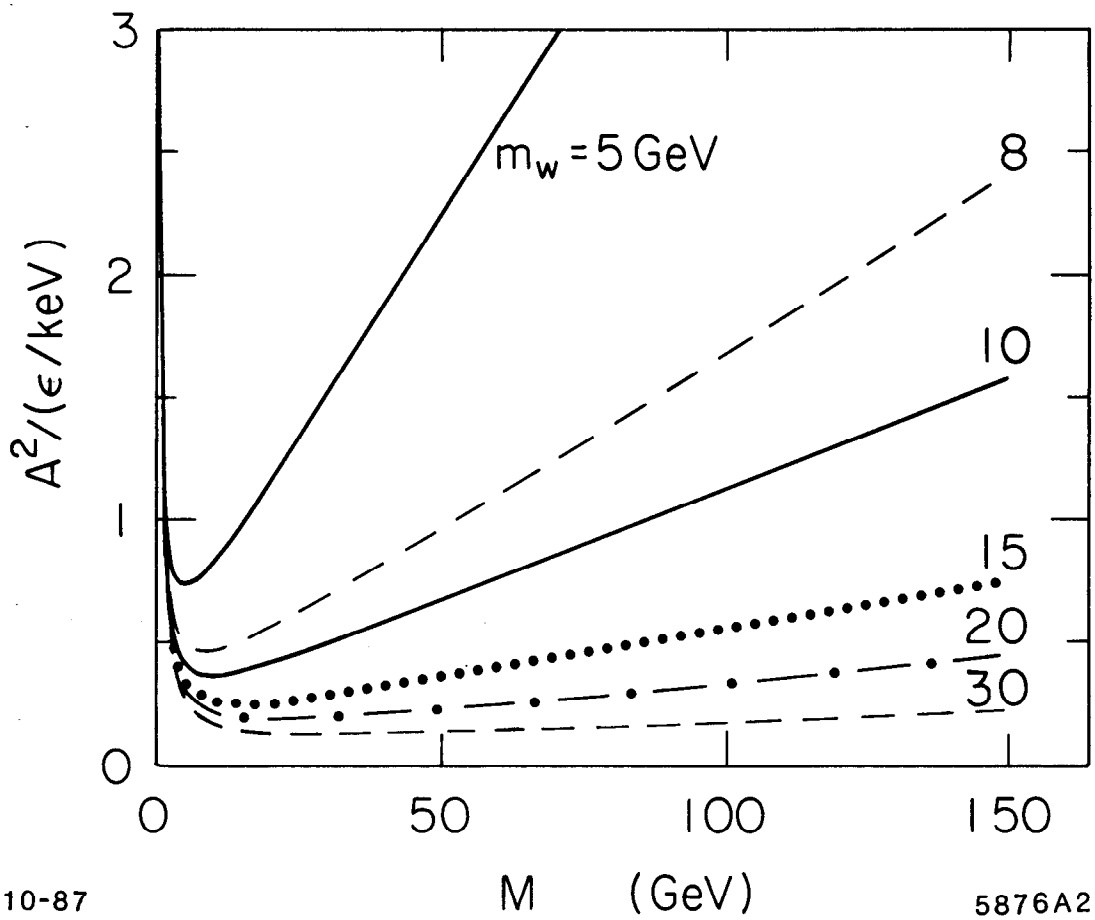
3
2
1
0
$A^2/(\epsilon/keV)$
$m_w = 5$ GeV
8
10
15
20
30
0
50
100
150
M (GeV)
10-87
5876A2

Fig. 2

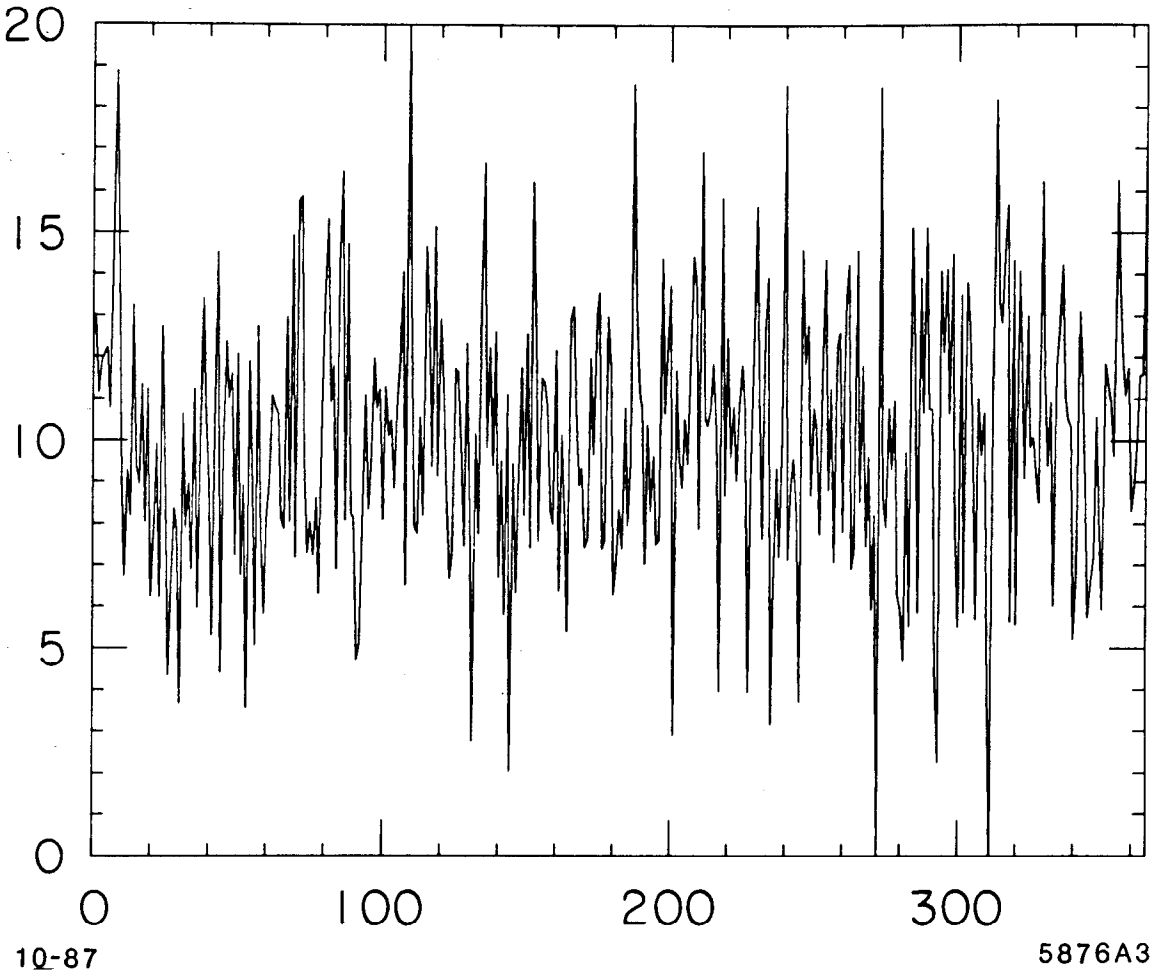

Fig. 3

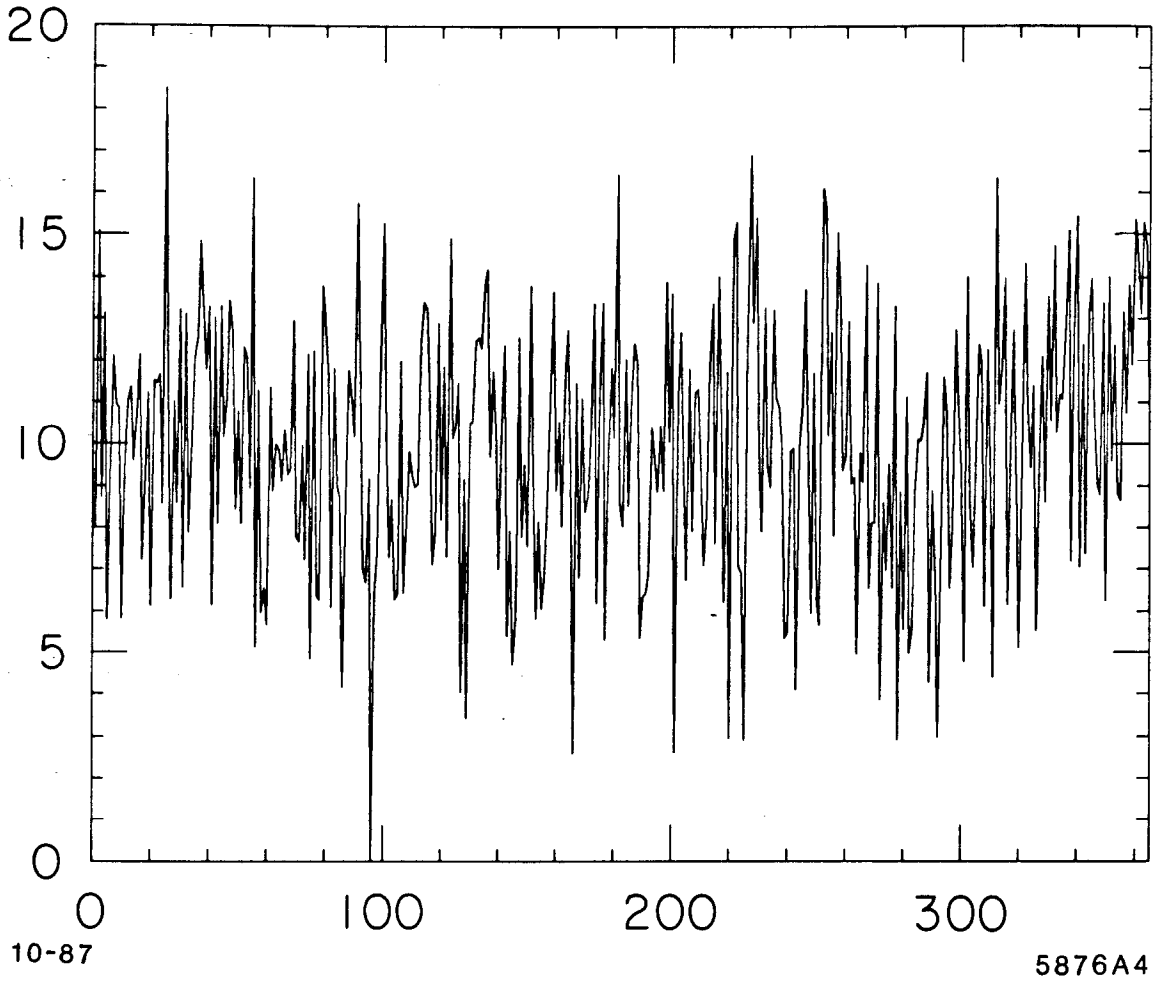

Fig. 4

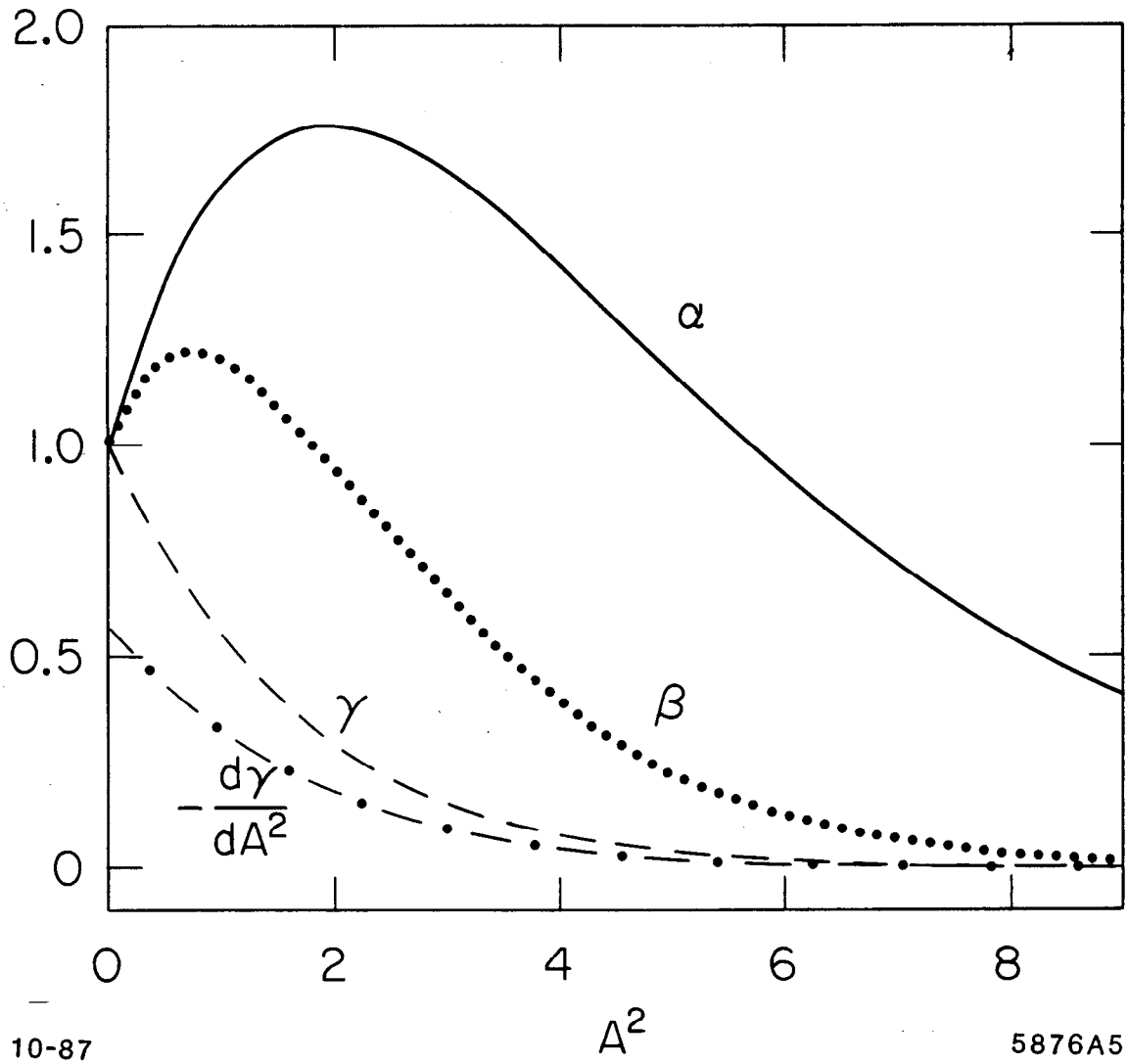

Fig. 5

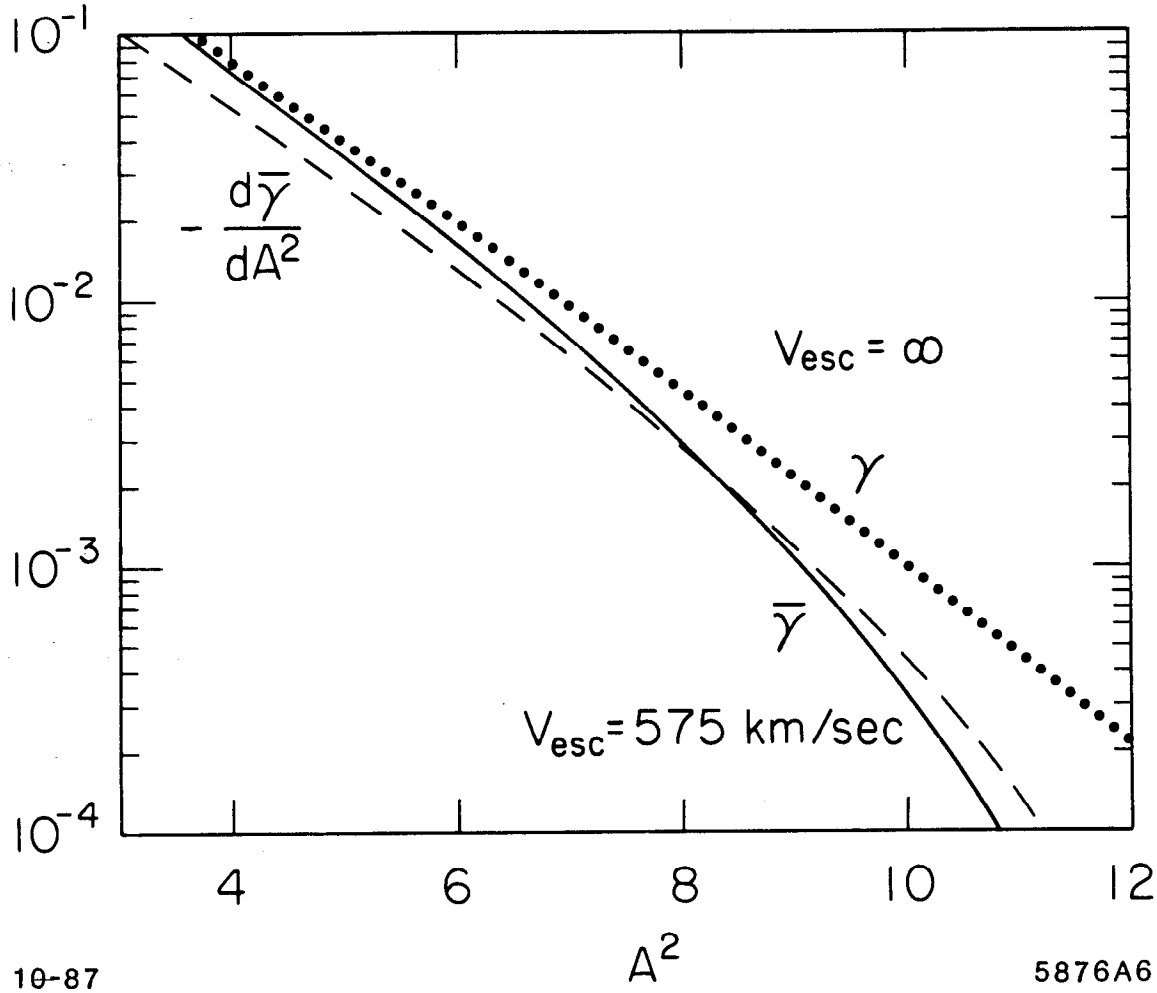
10^{-1}
10^{-2}
10^{-3}
10^{-4}
$-\frac{d\bar{\gamma}}{dA^2}$
$V_{esc} = \infty$
γ
$\bar{\gamma}$
$V_{esc} = 575$ km/sec
4
6
8
10
12
A^2
10-87
5876A6

Fig. 6

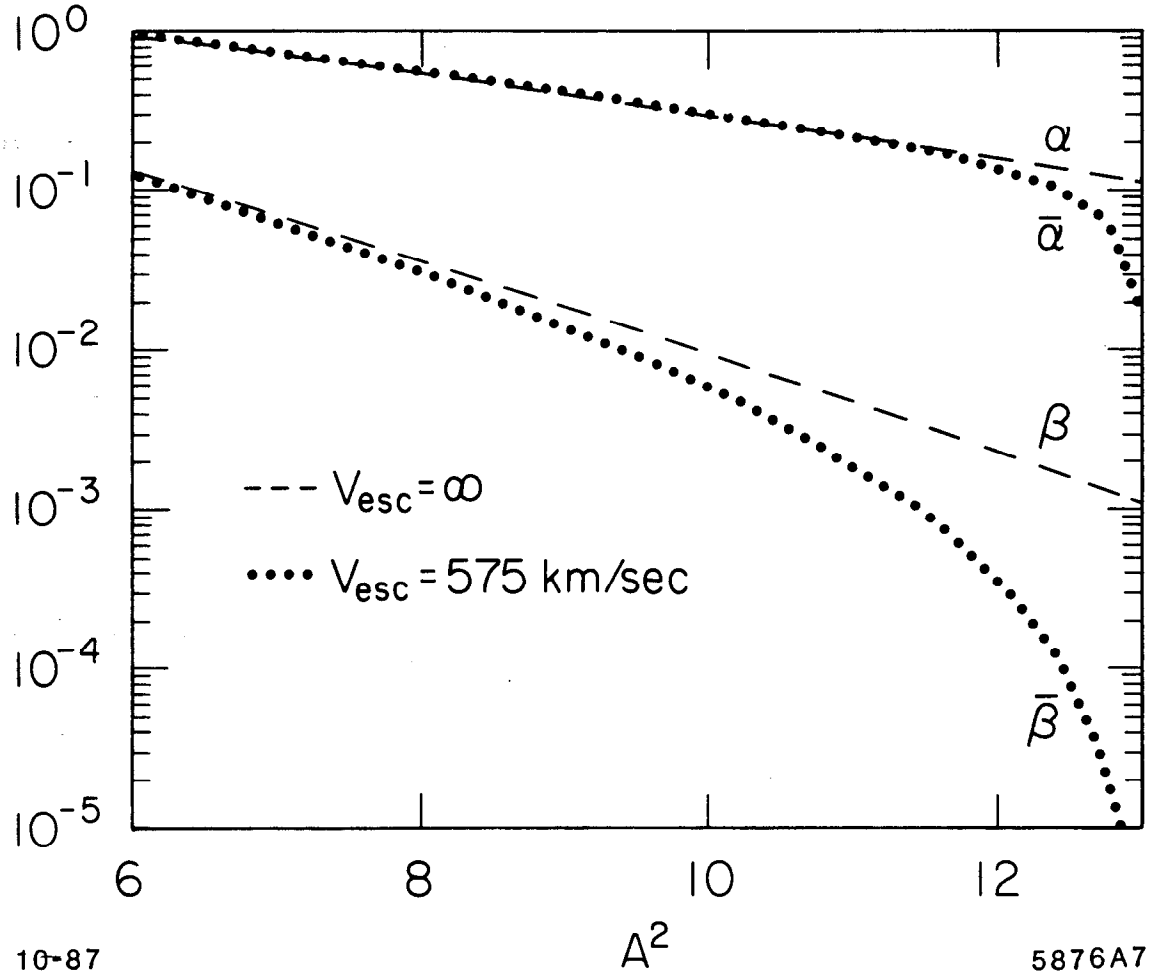
10^0
10^{-1}
10^{-2}
10^{-3}
10^{-4}
10^{-5}
6
8
10
12
A^2
α
$\bar{\alpha}$
β
$\bar{\beta}$
--- $V_{esc} = \infty$
•••• $V_{esc} = 575$ km/sec
10-87
5876A7

Fig. 7

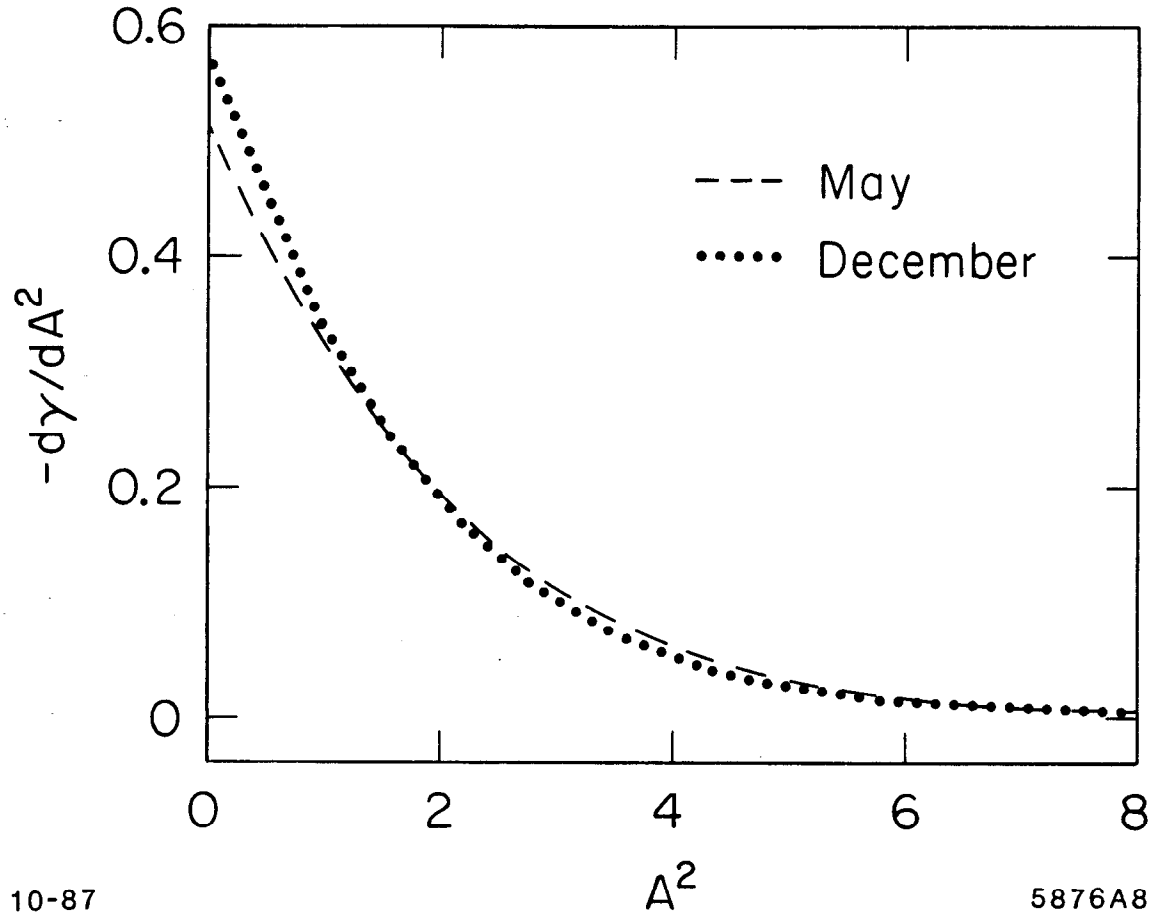

Fig. 8

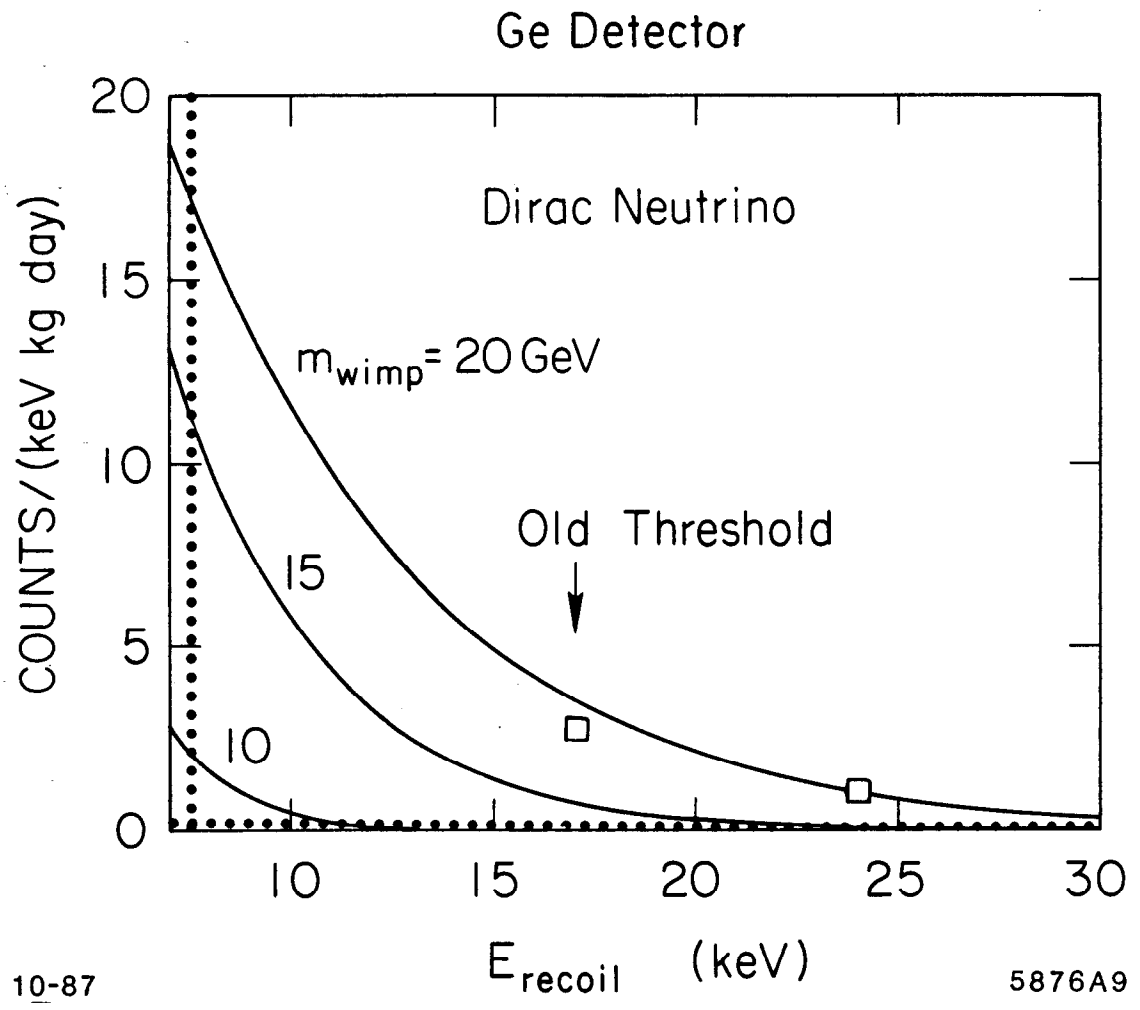
Ge Detector
Dirac Neutrino
m_{wimp}= 20 GeV
15
10
Old Threshold
COUNTS/(keV kg day)
0
5
10
15
20
10
15
20
25
30
E_{recoil} (keV)
10-87
5876A9

Fig. 9

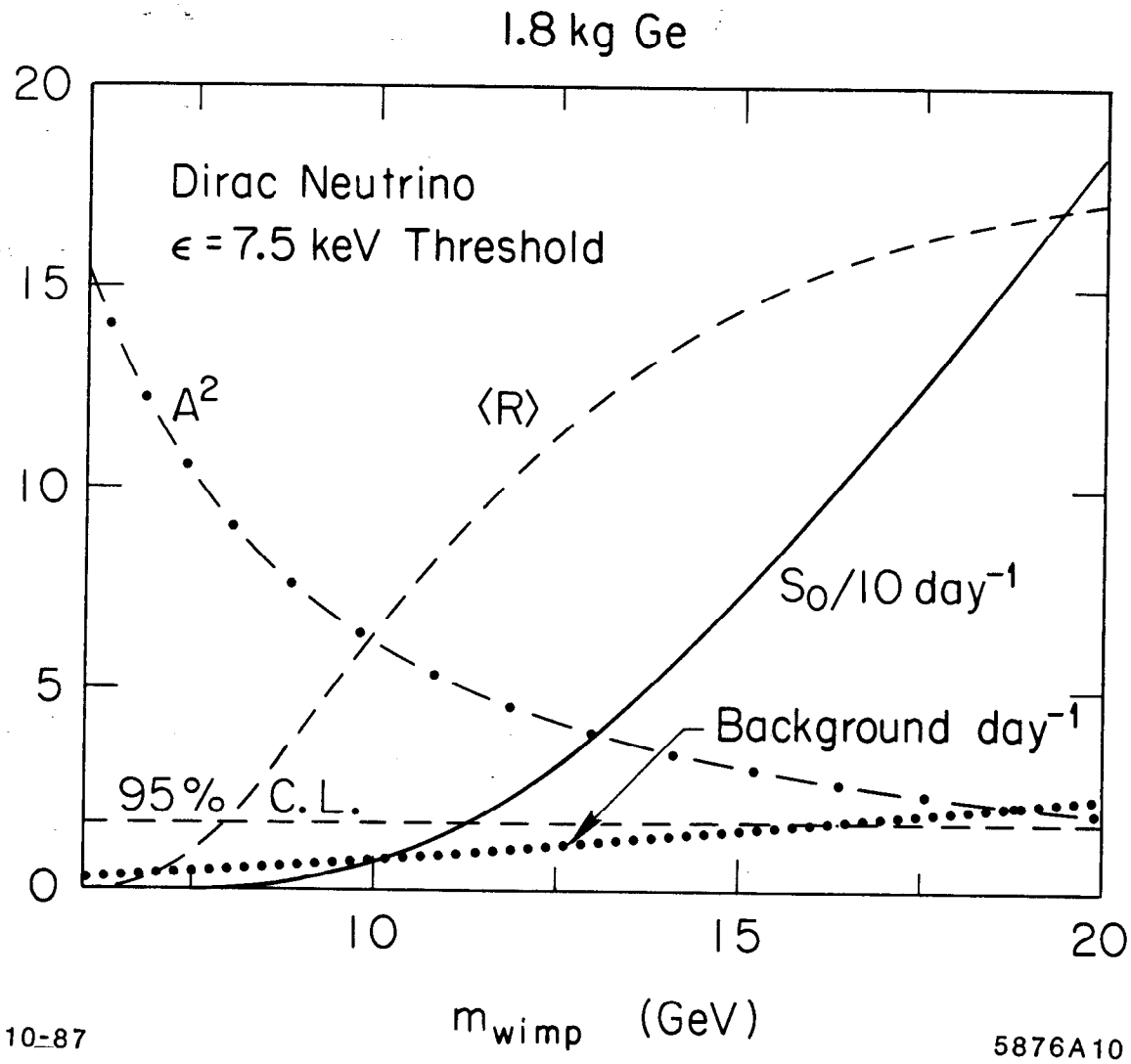
1.8 kg Ge
Dirac Neutrino
ϵ = 7.5 keV Threshold
A²
⟨R⟩
S₀/10 day⁻¹
Background day⁻¹
95% C.L.
20
15
10
5
0
10
15
20
m_wimp (GeV)
10-87
5876A10

Fig. 10

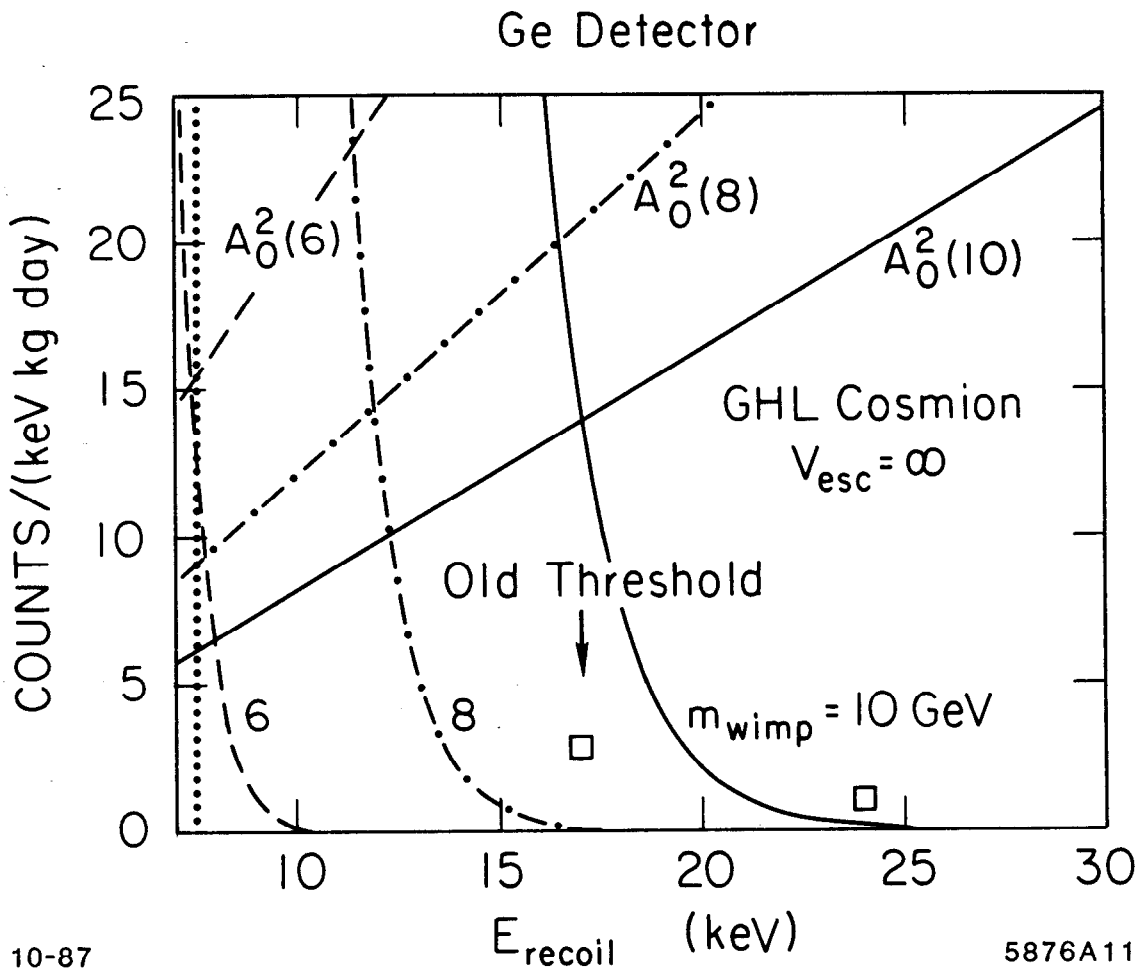
Ge Detector
COUNTS/(keV kg day)
25
20
15
10
5
0
10
15
20
25
30
E_{recoil} (keV)
$A_0^2(6)$
$A_0^2(8)$
$A_0^2(10)$
GHL Cosmion
$V_{esc} = \infty$
Old Threshold
6
8
m_{wimp} = 10 GeV
10-87
5876A11

Fig. 11

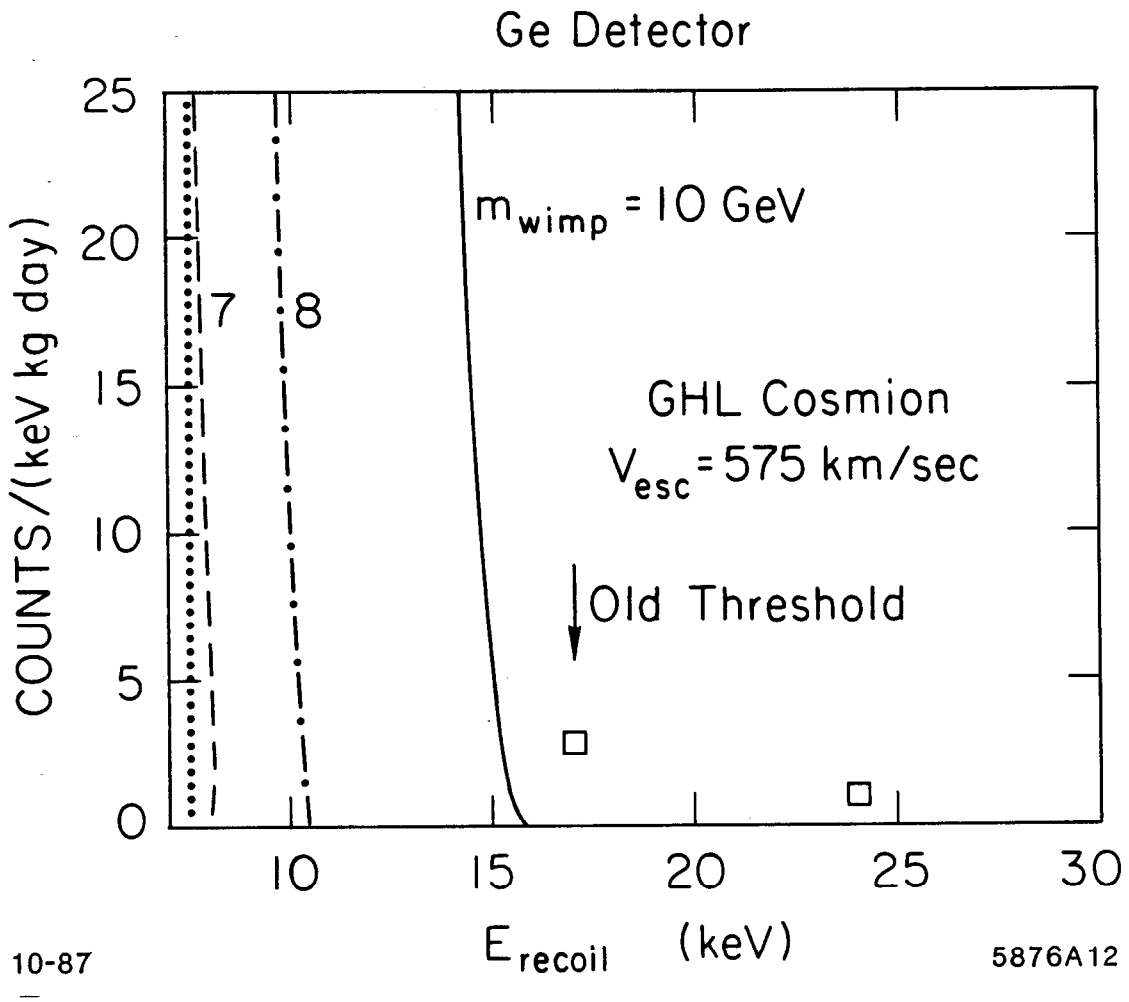
Ge Detector
COUNTS/(keV kg day)
25
20
15
10
5
0
7
8
m_{wimp} = 10 GeV
GHL Cosmion
V_{esc} = 575 km/sec
Old Threshold
10
15
20
25
30
E_{recoil} (keV)
10-87
5876A12

Fig. 12

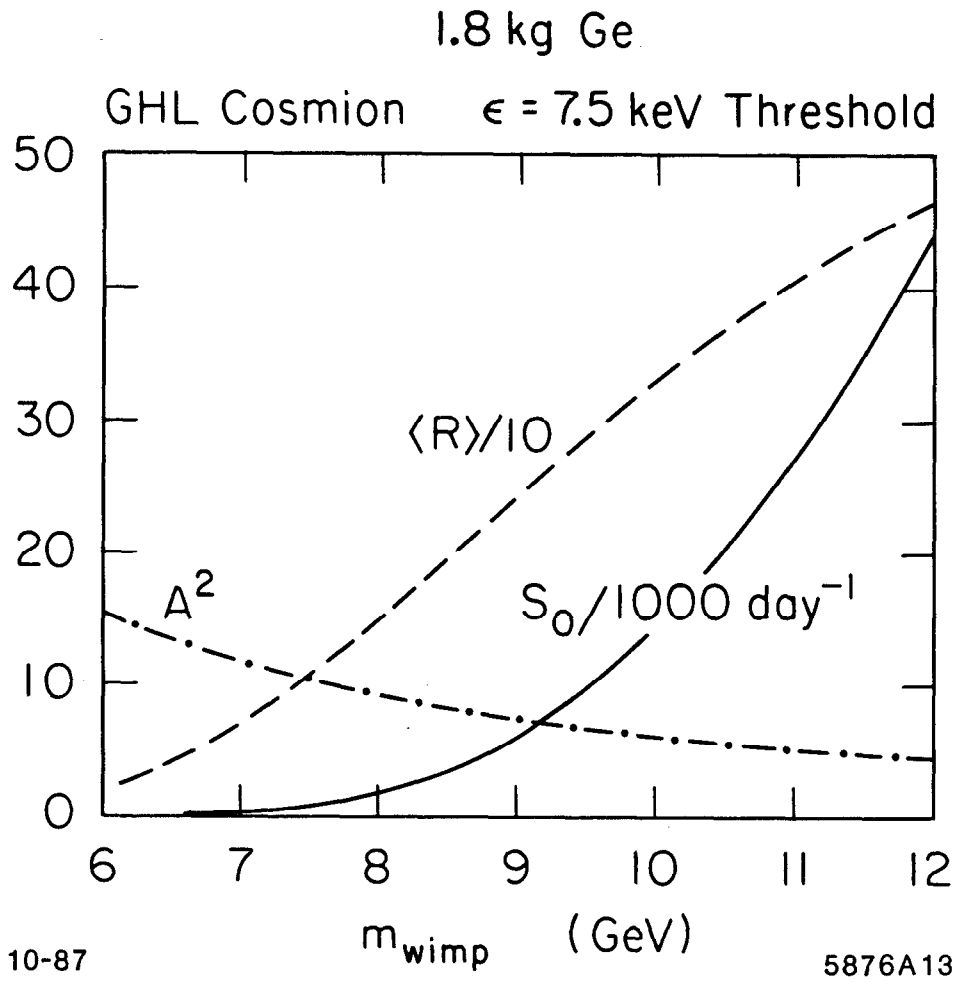
1.8 kg Ge
GHL Cosmion
ϵ = 7.5 keV Threshold
50
40
30
20
10
0
⟨R⟩/10
A²
S₀/1000 day⁻¹
6
7
8
9
10
11
12
m_wimp (GeV)
10-87
5876A13

Fig. 13

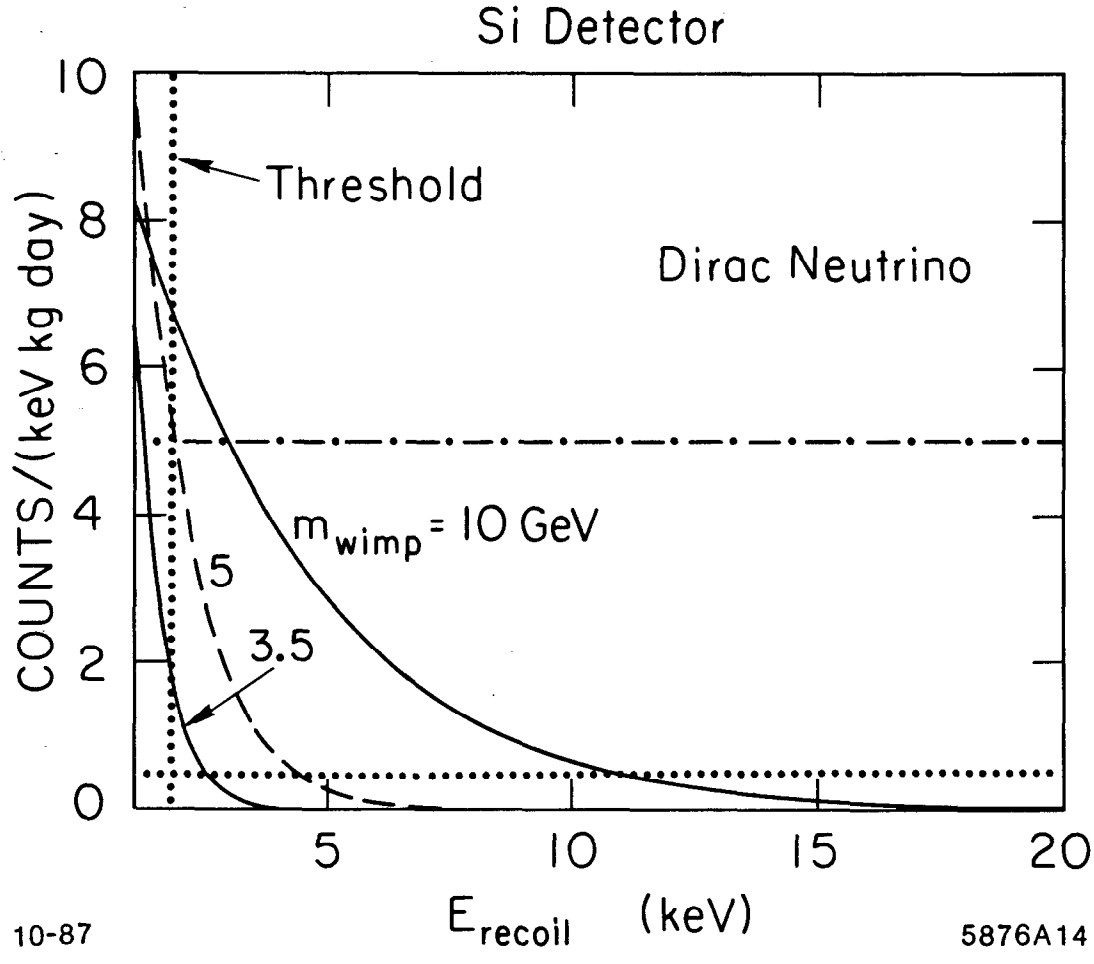
Si Detector
Threshold
Dirac Neutrino
m_{wimp} = 10 GeV
15
3.5
COUNTS/(keV kg day)
0
2
4
6
8
10
5
10
15
20
E_{recoil} (keV)
10-87
5876A14

Fig. 14

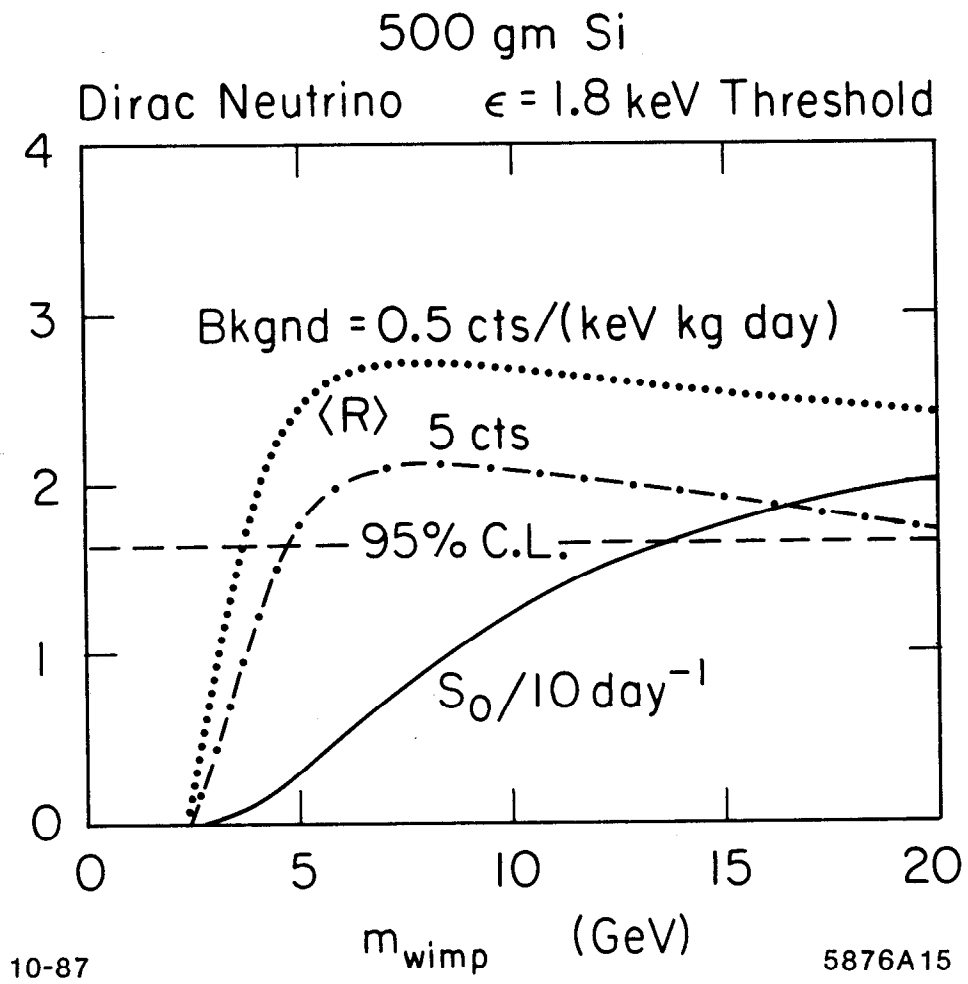
500 gm Si
Dirac Neutrino
ϵ = 1.8 keV Threshold
Bkgnd = 0.5 cts/(keV kg day)
⟨R⟩
5 cts
95% C.L.
S0/10 day⁻¹
0
1
2
3
4
0
5
10
15
20
mwimp (GeV)
10-87
5876A15

Fig. 15

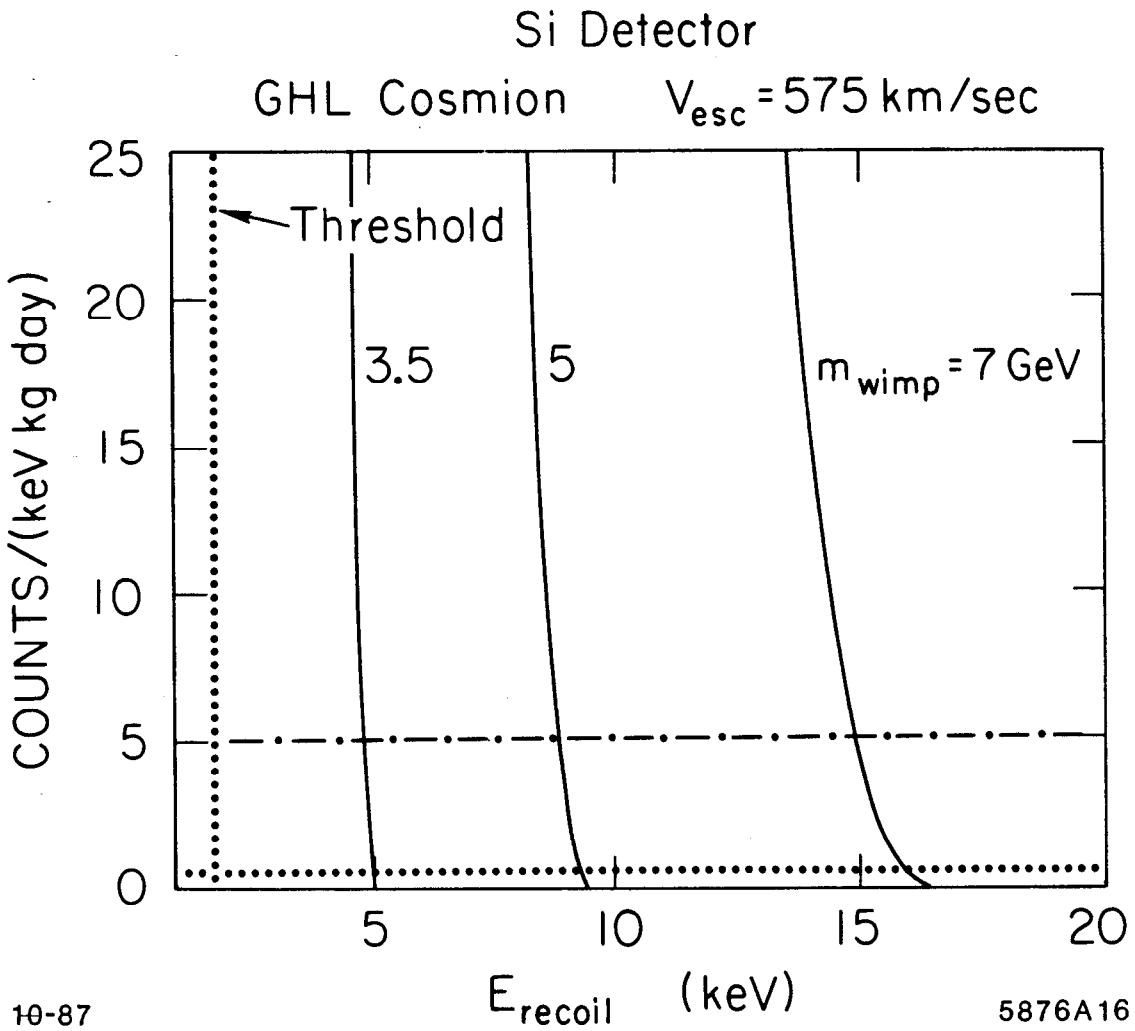
Si Detector
GHL Cosmion
V_{esc} = 575 km/sec
Threshold
3.5
5
m_{wimp} = 7 GeV
COUNTS/(keV kg day)
25
20
15
10
5
0
5
10
15
20
E_{recoil} (keV)
10-87
5876A16

Fig. 16

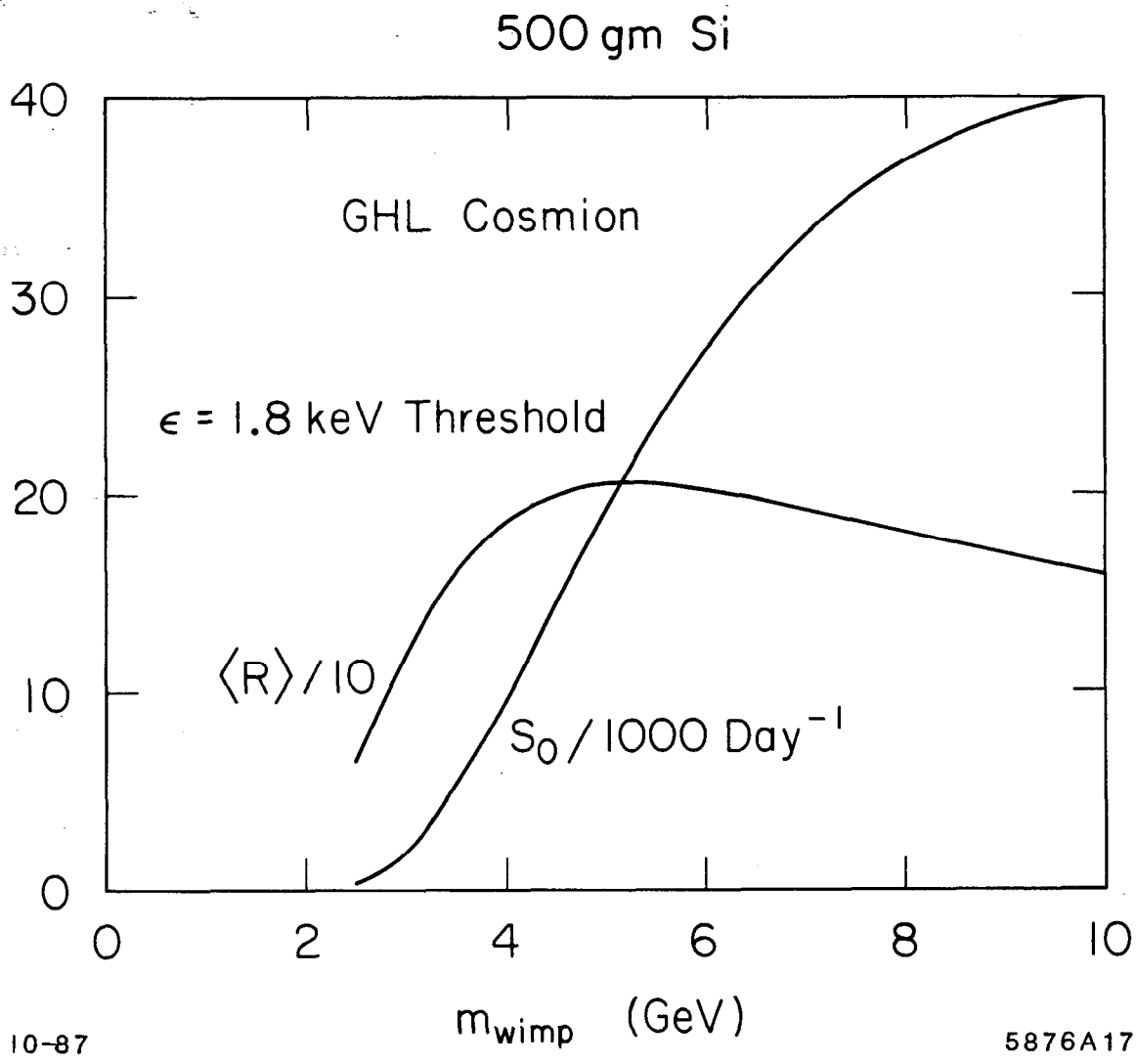
500 gm Si
GHL Cosmion
ϵ = 1.8 keV Threshold
⟨R⟩/10
S0 / 1000 Day⁻¹
40
30
20
10
0
0
2
4
6
8
10
mwimp (GeV)
10-87
5876A17

Fig. 17

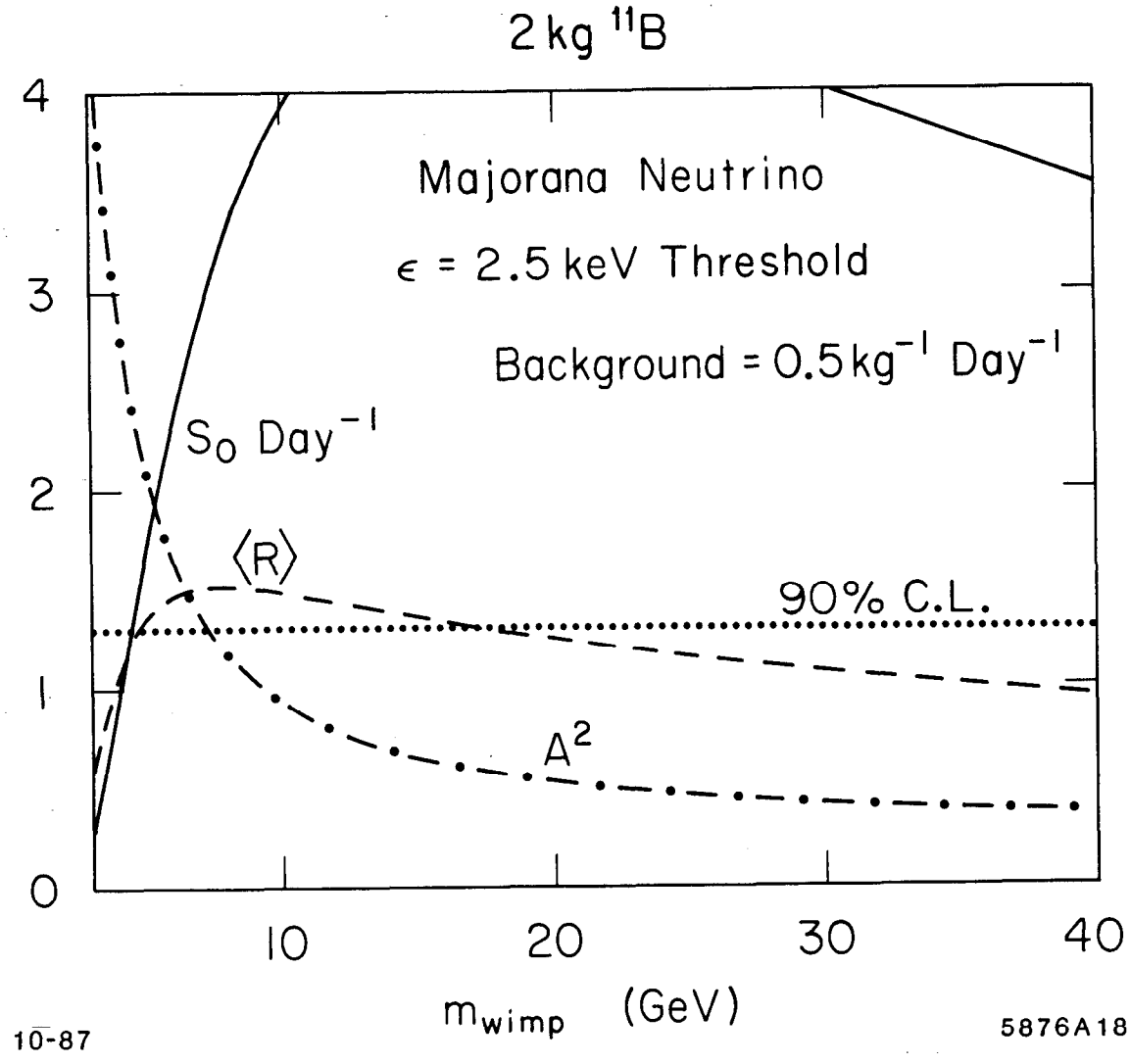
2 kg ^{11}B
Majorana Neutrino
ϵ = 2.5 keV Threshold
Background = 0.5 kg^{-1} Day^{-1}
S_0 Day^{-1}
$\langle R \rangle$
90% C.L.
A^2
0
1
2
3
4
10
20
30
40
m_{wimp} (GeV)
10-87
5876A18

Fig. 18

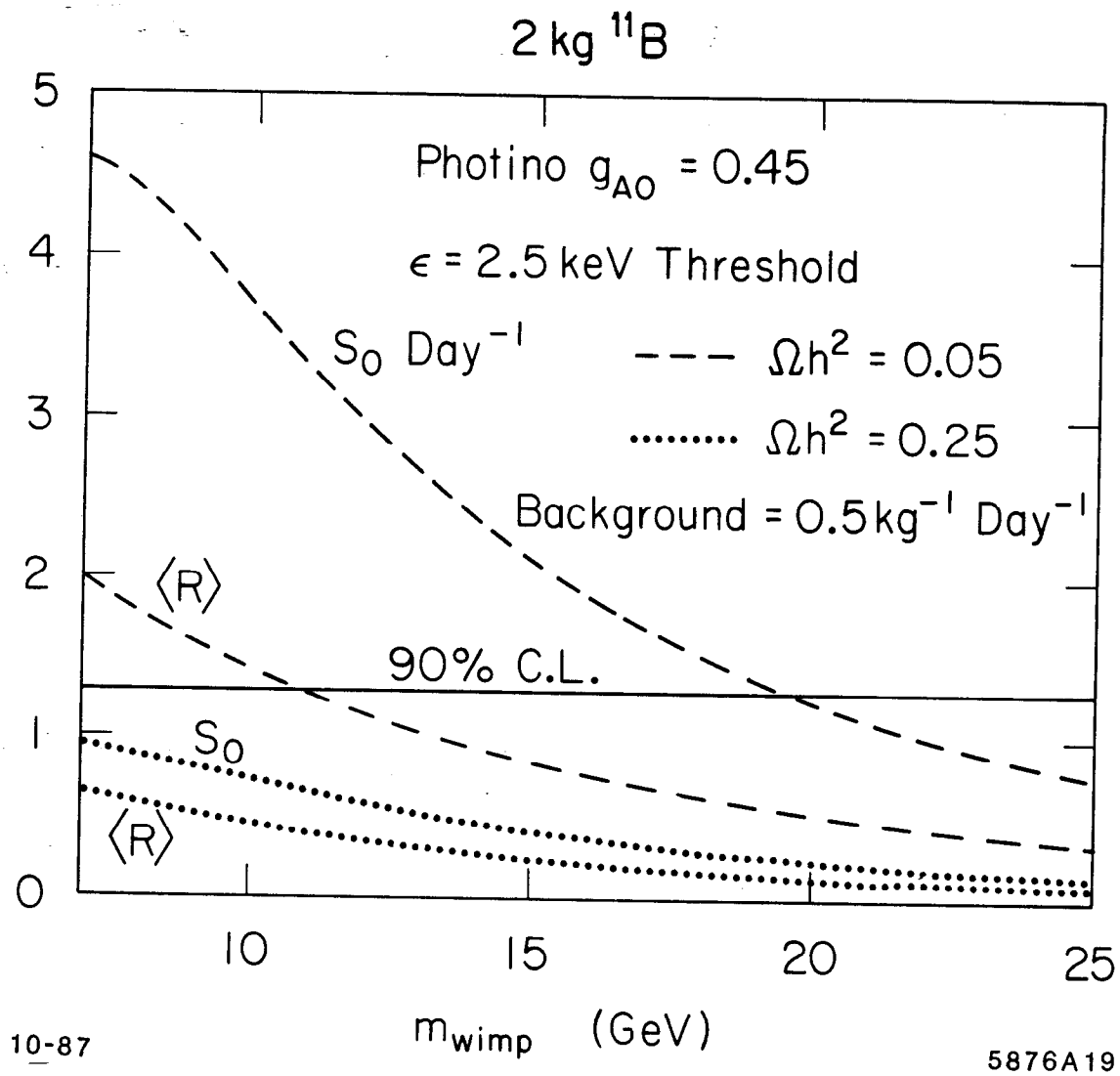
2 kg ^{11}B
Photino g_{AO} = 0.45
ϵ = 2.5 keV Threshold
S_0 Day^{-1}
Ωh^2 = 0.05
Ωh^2 = 0.25
Background = 0.5 kg^{-1} Day^{-1}
$\langle R \rangle$
90% C.L.
S_0
$\langle R \rangle$
0
1
2
3
4
5
10
15
20
25
m_{wimp} (GeV)
10-87
5876A19

Fig. 19

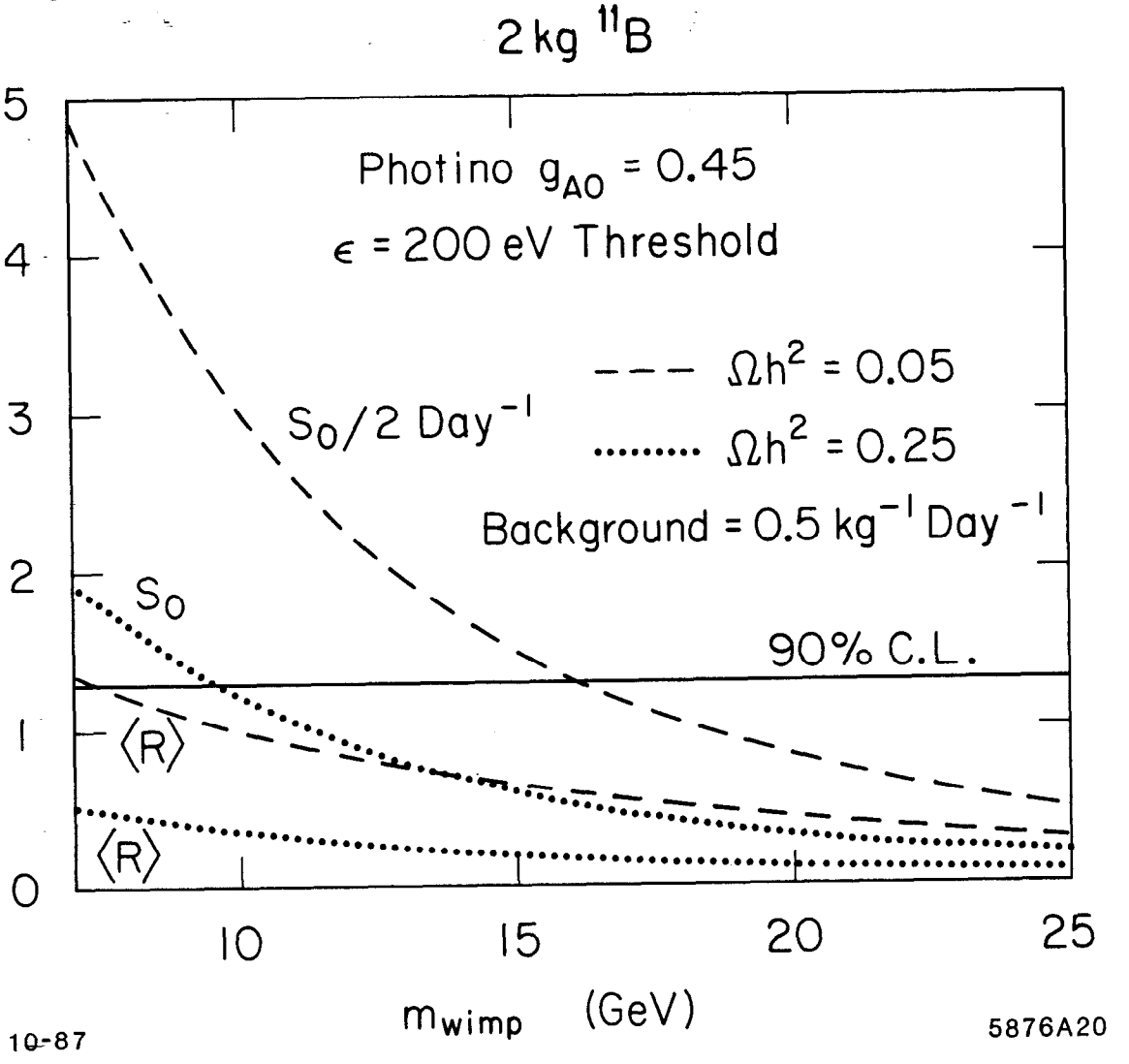
2 kg ^{11}B
Photino g_{A0} = 0.45
ϵ = 200 eV Threshold
Ωh^2 = 0.05
Ωh^2 = 0.25
$S_0/2$ Day^{-1}
Background = 0.5 kg^{-1} Day^{-1}
S_0
90% C.L.
$\langle R \rangle$
$\langle R \rangle$
0
1
2
3
4
5
10
15
20
25
m_{wimp} (GeV)
10-87
5876A20

Fig. 20

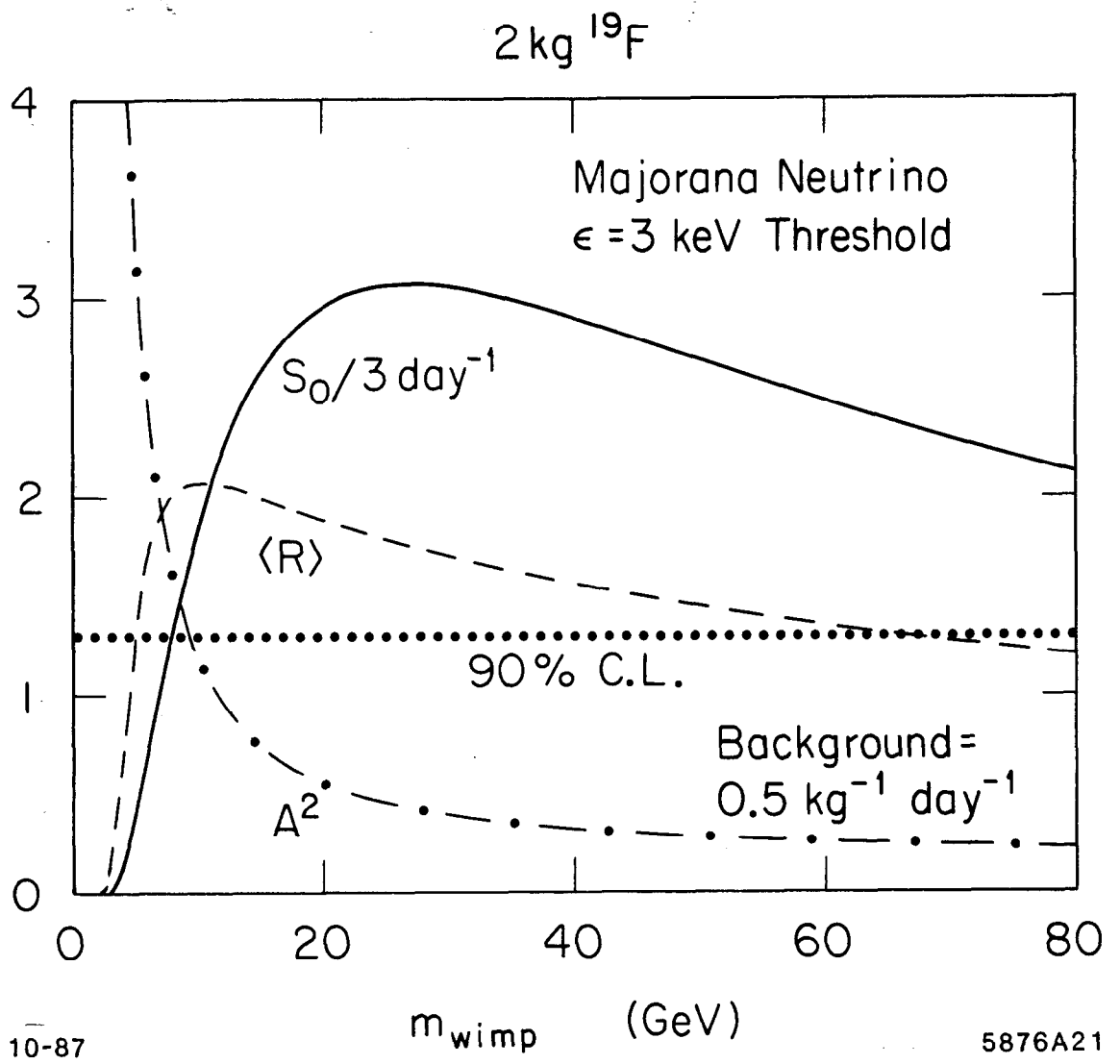
2 kg ^{19}F
Majorana Neutrino
ϵ = 3 keV Threshold
S_0/3 day^{-1}
⟨R⟩
90% C.L.
Background =
0.5 kg^{-1} day^{-1}
A^2
0
1
2
3
4
0
20
40
60
80
m_{wimp} (GeV)
10-87
5876A21

Fig. 21

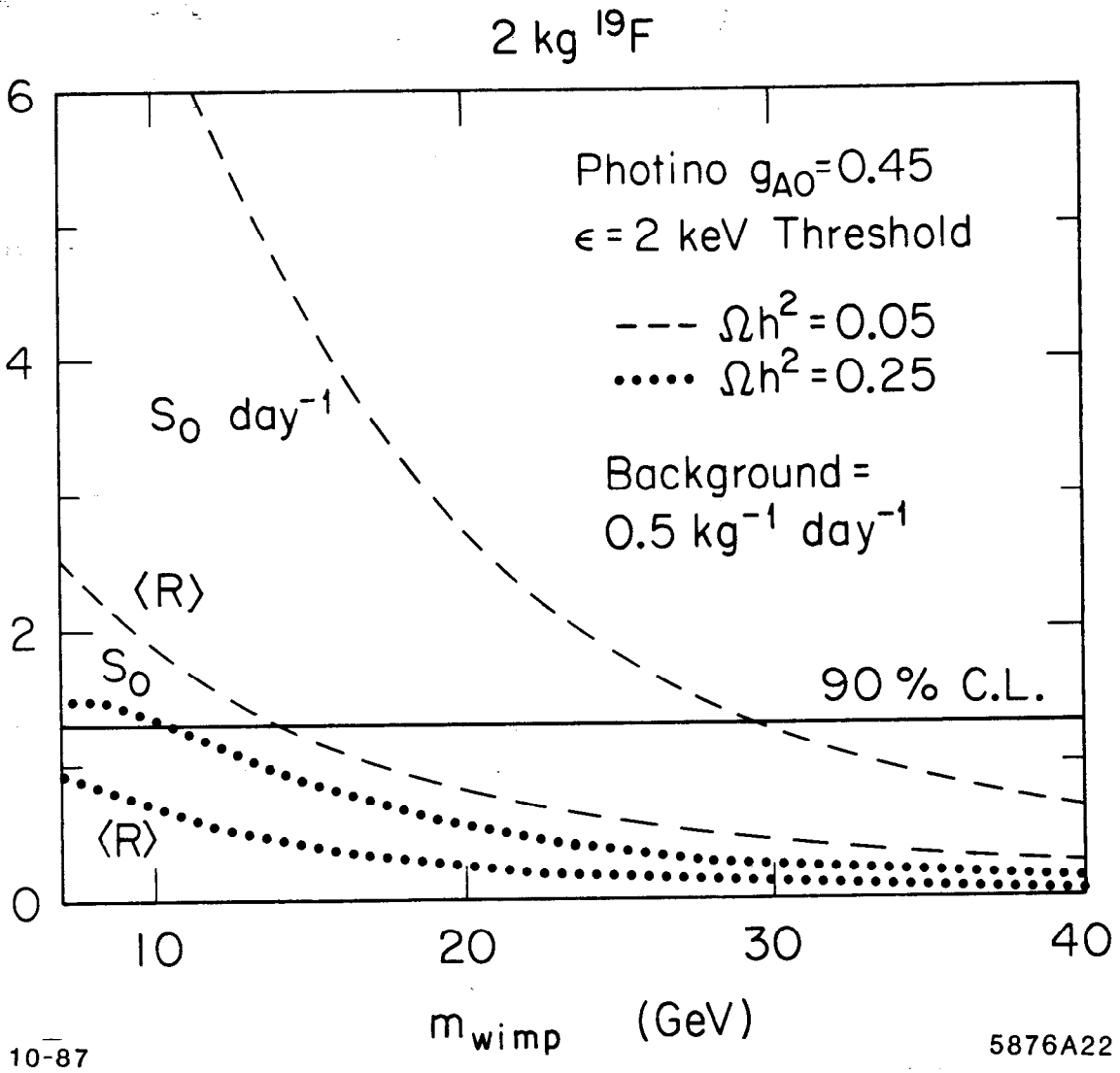
2 kg ^{19}F
Photino g_{A0}=0.45
ϵ = 2 keV Threshold
--- Ωh^2 = 0.05
••••• Ωh^2 = 0.25
Background =
0.5 kg^{-1} day^{-1}
S_0 day^{-1}
⟨R⟩
S_0
⟨R⟩
90 % C.L.
0
2
4
6
10
20
30
40
m_{wimp} (GeV)
10-87
5876A22

Fig. 22

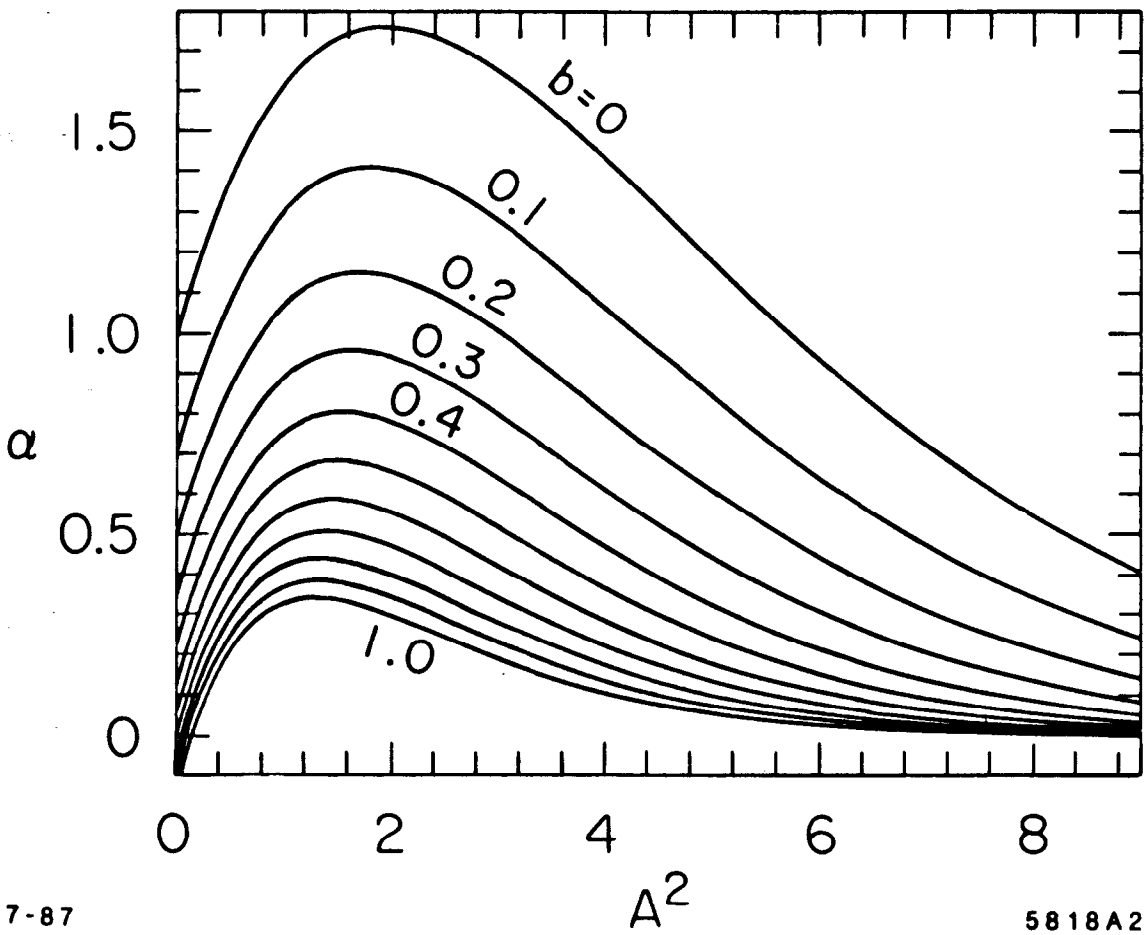

Fig 23